Elucidating Fibroblast Growth Factor-induced kinome dynamics using targeted mass spectrometry and dynamic modeling

Tim S. Veth[1,2], Chiara Francavilla[3], Albert J.R. Heck[1,2], Maarten Altelaar[1,2]*

1. Biomolecular Mass Spectrometry and Proteomics, Bijvoet Center for Biomolecular Research and Utrecht Institute for Pharmaceutical Sciences, University of Utrecht, Padualaan 8, Utrecht, 3584 CH, The Netherlands

2. Netherlands Proteomics Center, Padualaan 8, Utrecht, 3584 CH, The Netherlands

3. Division of Molecular and Cellular Function, School of Biological Science, and Manchester Breast Centre, Manchester Cancer Research Centre, Faculty of Biology Medicine and Health (FBMH), The University of Manchester, M139PT, Manchester, UK

*corresponding author

E-mail address of the corresponding author: m.altelaar@uu.nl

Summary

Fibroblast growth factors (FGFs) are paracrine or endocrine signaling proteins that, activated by their ligands, elicit a wide range of health and disease-related processes, such as cell proliferation and the epithelial-to-mesenchymal transition (EMT). The detailed molecular pathway dynamics that coordinate these responses have remained to be determined. To elucidate these, we stimulated MCF-7 breast cancer cells with either FGF2, FGF3, FGF4, FGF10, or FGF19. Following activation of the receptor, we quantified the kinase activity dynamics of 44 kinases using a targeted mass spectrometry assay. Our system-wide kinase activity data, supplemented with (phospho)proteomics data, reveal ligand-dependent distinct pathway dynamics, elucidate the involvement of not earlier reported kinases such as MARK, and revise some of the pathway effects on biological outcomes. In addition, logic-based dynamic modeling of the kinome dynamics further verifies the biological goodness-of-fit of the predicted models and reveals tight regulation of the RAF kinase family.

Keywords

Phosphoproteomics; kinase; targeted mass spectrometry; kinase dynamics; fibroblast growth factors; dynamic modeling; fibroblast growth factor receptor; breast cancer.

Introduction

Fibroblast growth factors (FGFs) and co-factors heparin/heparin-sulfate or beta-klotho induce trans-autophosphorylation upon binding to fibroblast growth factor receptors (FGFRs), thereby activating signaling pathways and regulating diverse biological processes (Ornitz & Itoh, 2022; Sarabipour & Hristova, 2016; Su et al., 2014) (Kuro-o, 2019; Spivak-Kroizman et al., 1994). There are 18 FGF ligands known so far that can activate the 7 alternatively spliced isoforms of 4 FGFR genes. Specific combinations of receptor and ligand result in the regulation of a plethora of diverse cellular processes, including cell differentiation, cell proliferation, and epithelial-mesenchymal transition (EMT) (Chen, 2005; Xie et al., 2020).

Besides the role of FGFs in health, during development and adult life, dysregulated FGF-FGFR signaling is implicated in various types of cancer, including breast cancer (Francavilla & O'Brien, 2022; Korc & Friesel, 2009; Presta et al., 2017; Y. Zhou et al., 2020). FGF2 is commonly detected in the tumor microenvironment of breast cancer and can induce tumor growth (Giulianelli et al., 2019; Sharpe et al., 2011). FGF3, FGF4, and FGF19 are located on the 11q13 amplicon, which is amplified in 15-20% of breast cancer patients and are all linked to increased tumor progression (Karlsson et al., 2011, p. 201; W. Wang et al., 2015; C. Zhang et al., 2020; Zhao et al., 2018). FGF10 can drive type III EMT in breast cancer, promoting invasiveness (Abolhassani et al., 2014). These unfavorable effects in breast cancer patients result from diverse and complex FGF-driven cellular signaling (Presta et al., 2017).

The fine-tuned coordination of the diverse FGF-driven cellular processes is thought to be regulated by the MAPK/ERK pathway, the PI3K pathway, the PLCγ pathway, and the JAK-STAT pathway (Dailey et al., 2005; Ferguson et al., 2021) (Ornitz et al., 1996; Touat et al., 2015; X. Zhang et al., 2006). For example, the MAPK/ERK pathway is thought to drive cell proliferation, and the PI3K pathway is believed to regulate EMT (Katoh & Nakagama, 2014; Tomita et al., 2021). These pathways are highly dependent on multiple kinases that relay signals by adding phosphate groups to proteins or other molecules. Kinase activity is often determined by phosphorylation in the kinase activation loop, which can be measured and quantified using a targeted mass spectrometry based kinome assay (Nolen et al., 2004; Schmidlin et al., 2019). Even though the main pathways involved in FGF signaling are elucidated, molecular mechanistic

insights into the regulations of the differential cellular processes are still largely lacking (Gurzu et al., 2019; Ramos et al., 2010).

FGF2, FGF3, FGF4, FGF10, and FGF19 are all associated with breast cancer, however, insights into the differential signaling of these FGFs are lacking. It is unclear what pathways and kinases are regulated by the different FGFs. Also, no mechanistic signaling comparisons are investigated to elucidate the importance of each of the FGFs and their possible roles in breast cancer. Gaining these biological insights is key to understanding the implications of FGF signaling in breast cancer.

Here, we aim to broaden our understanding of FGF signaling by quantifying temporal kinase activation dynamics using a selected reaction monitoring assay (SRM) with broad coverage of kinases that are involved in the FGFR signaling pathway. To verify the biological results from the longitudinal SRM data, we created a dynamic mechanistic model of the signaling pathway using logic-based ordinary differential equations. To explain discrepancies in our developed model, we used modeling-guided analysis of shotgun phosphoproteomics data. Our approach successfully mapped FGF2, FGF3, FGF4, FGF10, and FGF19 signaling in breast cancer cell lines and allowed us to add hitherto unknown involved kinases and signaling dynamics to FGF stimulations.

Methods

Cell culture

MCF-7 (ATCC), BT-474 (ATCC), and EFM-192a (DSMZ) cells were grown in Dulbecco's modified Eagle's medium (DMEM) supplemented with 10% FBS (Sigma) and 2mM glutamine. Cells were regularly tested for mycoplasma. All cells were cultured in a humidified incubator equilibrated with 5% CO2 at 37 °C. Experiments were performed after the 5th passage and before the 20th passage to limit cell heterogeneity between experiments.

Sample preparation for mass spectrometry

For mass spectrometry experiments, ~5 million cells were plated in triplicates in 10cm plates in regular medium. After 24 hours, the medium was changed to serum-starved medium supplemented with 5 µg/mL heparin (Thermo Scientific). After 24 hours, cells were incubated with 50 ng/mL of either FGF2 (Peprotech), FGF3 (KyvoBio), FGF4 (Peprotech), FGF10

(Peprotech), or FGF19 (Peprotech). Cells were washed three times with ice-cold PBS, scraped, and snap-frozen until further sample preparation.

Cell growth assay

Triplicate groups of ~0.1 million cells were plated in 12 well-plates again first in regular medium and subsequently in medium with either 5 µg/mL heparin or without. After 24 hours, one of the 5 different FGF ligands was added, and the plate was incubated in an IncuCyte ZOOM™ at 37 °C/5% CO2 until the end of the experiment. Pictures of each well were taken every hour, of which the percentage plate coverage was determined. Significance between groups was determined using an ANOVA and Tukey's range test ($p < 0.05$).

Scratch wound healing assay

In 12 well plates, triplicates of 3e5 cells were plated in a regular medium, after 24 hours, the medium was changed to starved medium supplemented with 5 µg/mL heparin. Subsequently, the cells were verified to be confluent when the scratch assay was performed (Liang et al., 2007). The scratch assay was analyzed as described before (Suarez-Arnedo et al., 2020). In short, using the ImageJ/Fiji script "Wound Healing Size Tool", the percentage of wound closure was calculated between t = 24h and t = 0 (Schindelin et al., 2012). Significance between groups was determined using an ANOVA and Tukey's range test (biological triplicates, $p < 0.05$).

Spectral library generation

Spectral libraries were used to determine peptide fragmentation characteristics and their indexed retention time, which are key for identifying peptides in the tier 2 SRM assay. The custom mix of heavy labeled peptides (JPT or ThermoFisher Scientific) was mixed with iRT peptides (Biognosys) and analyzed using an Orbitrap Q-Exactive HF (ThermoFisher Scientific). An unscheduled parallel reaction monitoring (PRM) method scanned for the +2 and +3 charged peptides, including all possible methionine oxidations. Peptides were separated using a 2 h gradient a 120k resolution was used for the PRM assay, resulting in a minimum of 5 spectra per peptide. Raw files were analyzed using MaxQuant (version 1.6.10.43), carbamidomethyl cysteine as fixed modification, and the variable modifications serine/threonine/tyrosine phosphorylation, methionine oxidation, and isotope labels. The search results were filtered using a 1% FDR cut-off, and subsequently, using Skyline (version 20.1.1.83), pseudo-MS2 spectra were generated, which were used as the peptide library.

SRM assay development

The SRM assay was developed using previously described methods (Schmidlin et al., 2019). The assay was developed on a TSQ Altis (ThermoFisher Scientific). In brief, the 10 most intense fragment ions from the library were used as initial transitions. These transitions were used to optimize multiple parameters, such as retention time and collision energy. The collision energy was optimized per transition using Skyline, with the TSQ Vantage CE formula as starting point (CE = 0.03 m/z + 2.905 for doubly charged precursors and CE = 0.038 m/z + 2.281 for precursor charges of three and higher) and optimized using steps of 1 voltage.

Protein digestion selected reaction monitoring assay

Snap-frozen protein pellets were lysed, reduced, and alkylated in lysis buffer (1% sodium deoxycholate (SDC), 10 mM tris(2-carboxyethyl)phosphine hydrochloride (TCEP)), 40 mM chloroacetamide (CAA), and 100 mM TRIS, pH 8.0 supplemented with phosphatase inhibitor (PhosSTOP, Roche) and protease inhibitor (cOmplete mini EDTA-free, Roche). Cells were heated at 95C and sonicated with a Bioruptor Plus (Diagenode) for 15 cycles of 30 s. Bradford protein assay (Bio-Rad Protein Assay Kit I, Bio-Rad) was used to determine the protein amount, after which samples were split into 200µg aliquots. Proteins were digested overnight at 37C with trypsin (1:50 µg/µg) (Sigma-Aldrich) and lysyl endopeptidase (1:75 µg/µg) (Wako). Heavy labeled phosphopeptides were added to the samples. The SDC was precipitated with 2% formic acid (FA) twice, after which samples were desalted and enriched in an automated fashion using the AssayMap Bravo platform (Agilent Technologies) with corresponding AssayMap C18 (Agilent Technologies) reverse-phase column as previously described (Post et al., 2017).

SRM LC-MS/MS Setup

Samples were analyzed on a TSQ Altis (Thermo Scientific) coupled to an UltiMate 3000 (Thermo Scientific), and an easy spray analytical column (ES802A, 25 cm, 75 mm ID PepMap RLSC, C18, 100 A˚, 2 mm particle size column (Thermo Scientific)). First, samples were reconstituted in 2% LC-MS grade formic acid. Samples were loaded on a trap column (Acclaim™ PepMap™ 100 C18 HPLC Column 0.3x5mm with 5 µm particles (Thermo Scientific)) with 2.2% Buffer A (0.1% FA) for 3 minutes and subsequently separated using 0-32% buffer B (99.9%ACN, 0.1%FA) in 35 min at 300nL/min and followed by a 20 min column wash with 80% buffer B at 300nL/min, and 10-minute column equilibration at 2.2% B. The TSQ

Altis spray voltage was set at 1.9 kV and fragmented at 1.5 mTorr in the second quadrupole. The first quadrupole was set at 0.7 da FWHM, and the third quadrupole at 1.2 da FWHM. All transitions were measured with optimized collision energy without scheduling and a cycle time of 1.5 sec.

SRM data assessment

All experiments were analyzed using Skyline-Daily (version 20.2.1.404) (Pino et al., 2020). The quality of the peptides was assessed mainly on the signal similarity between the heavy and the light peptides. The most important aspects were perfect co-elution, peak shape, and relative contributions of each transition between the heavy and the light peptide. A rdotp > 0.95 was maintained to indicate the similarity between the heavy and the light peptide. In-house R scripts were used for further data visualization and analysis.

Logic-based dynamic modeling

Logic-based dynamic modeling was performed as described earlier (Tognetti et al., 2021). In short, first, a prior knowledge network (PKN) was generated using Omnipath and converted to a simple interaction file (SIF) (Türei et al., 2016). Normalization was done per kinase across all the FGFs. The average fold change to t=0 was scaled between 0-1 using the 99% interquartile range (biological triplicates) described in **Equation 1**.

$$X = \frac{x - x_{.005}}{x_{.995} - x_{.005}}$$

Equation 1

Values < 0 or > 1 were set to 0 or 1, respectively. The different FGFs were set to 0.75 for their modeling.

The model was trained using the freely available CNORode for all FGFs simultaneously (Terfve et al., 2012). Each kinase can be described using a continuous update function B_i where the activity of a kinase x_i is predicted {0,1} using the associated upstream effectors, as shown in Equation 2 (Wittmann et al., 2009).

$$x_i = \tau_i(B_i\left(f(x_{1,i})f(x_{2,i}), \dots f(x_{n,i})\right) - x_i)$$

Equation 2

τ_i can be interpreted as the kinase responsiveness to upstream effectors where a small value indicates a slower response. Each transfer function is a Hill-type function, as previously described and presented in Equation 3 (Eduati et al., 2017).

$$f_{ij}(x) = 1 - \frac{(1-x)^{n_{ij}}}{(1-x)^{n_{ij}} - k_{ij}^{n_{ij}}} \left(1 + k_{ij}^{n_{ij}}\right)$$

Equation 3

The sigmoidal shape curve is determined by parameters n and k. The k parameter can be interpreted as the strength of the interaction where a high k value describes a high signal throughput.

Kinase dynamic parameter estimation

Each kinase is assigned a fixed n value of 3 and a k and τ value determined by the dynamic modeling. CNORode and the MEIGOR toolkit were used, which uses the normalized kinase activity data and the PKN to determine the best k and τ values based on the smallest root-mean-square error (RMSE) (Egea et al., 2014). The method entails L2 normalization to prevent overfitting, which was set to a value of 10^{-5}. The update function was verified to have achieved optimal performance based on the RMSE response curves. Model goodness of fit was determined using Pearson's r and the RMSE of all measured and predicted time points of all kinases. The biological RMSE was determined using the deviation between the measured values and the mean.

Peptide work-up untargeted phosphoproteomics

Peptide work-up was performed identically to the SRM peptide workup except that no heavy labeled peptides were added after digestion.

Peptide work-up untargeted proteomics

Snap-frozen protein pellets were lysed, reduced, and alkylated in lysis buffer (1% sodium deoxycholate (SDC), 10 mM tris(2-carboxyethyl)phosphine hydrochloride (TCEP)), 40 mM chloroacetamide (CAA), and 100 mM TRIS, pH 8.0 supplemented with protease inhibitor (cOmplete mini EDTA-free, Roche). Cells were heated at 95C and sonicated with a Bioruptor Plus (Diagenode) for 15 cycles of 30 s. Bradford protein assay (Bio-Rad Protein Assay Kit I, Bio-Rad) was used to determine the protein amount, after which samples were split into 10µg

aliquots. Proteins were digested overnight at 37C with 1:50 trypsin (Sigma-Aldrich) and 1:75 and lysyl endopeptidase (Wako), after which samples were desalted using an Oasis® platform, dried down, and stored at -80 until further use.

Data-dependent analysis of untargeted phosphoproteomics

Samples were suspended in 2% formic acid and analyzed on an Exploris (Thermo Scientific) coupled to an UltiMate 3000 (Thermo Scientific), fitted with a µ-precolumn (C18 PepMap100, 5µm, 100 Å, 5mm × 300µm; Thermo Scientific), and an analytical column (120 EC-C18, 2.7µm, 50cm × 75µm; Agilent Poroshell). Peptides are loaded in 9% Buffer A (0.1% FA) for 1 minute and separated using 9-36% buffer B (80%ACN, 0.1%FA) in 97 min at 300nL/min and followed by a 6 min column wash with 99% buffer B at 300nL/min, and a 10-minute column equilibration at 9% B. The MS was operated in DDA mode, with the MS1 scans in a range of 375-1600 m/z acquired at 60k, using an automatically set AGC target. MS2 scans were acquired with a 16s dynamic exclusion at a 30k resolution, 28% normalized collision energy, and an isolation window of 1.4 m/z.

Raw files were processed via MaxQuant version 1.6.17.0 using the verified human proteome from UniprotKB (release 09-2019) containing 20369 proteins (Tyanova et al., 2016). A maximum of 5 modifications and two miscleavages were set using fixed carbamidomethyl modification, and the variable modifications oxidized methionine, protein N-terminal acetylation, and serine/threonine/tyrosine phosphorylation. The protein and peptide false discovery rates were set to < 0.01 and conducted with match between runs enabled. No normalization or imputation was applied.

Shotgun proteomics analysis

Samples were suspended in 2% formic acid and analyzed on a Q-Exactive HF (Thermo Scientific) coupled to an UltiMate 3000 (Thermo Scientific), fitted with a µ-precolumn (C18 PepMap100, 5µm, 100 Å, 5mm × 300µm; Thermo Scientific), and an analytical column (120 EC-C18, 2.7µm, 50cm × 75µm; Agilent Poroshell). Peptides are loaded in 9% Buffer A (0.1% FA) for 1 minute and separated using 9-44% buffer B (80%ACN, 0.1%FA) in 155 min at 300nL/min and followed by a 6 min column wash with 95% buffer B at 300nL/min, and a 10-minute column equilibration at 9% B. The MS was operated in DDA mode, with the MS1 scans in a range of 375-1600 m/z acquired at 60k, using an AGC target of 3e6. MS2 scans were

acquired with a 24s dynamic exclusion at a 30k resolution, 27% normalized collision energy, and an isolation window of 1.4 m/z.

Raw files were processed via MaxQuant version 1.6.17.0 using the verified human proteome from UniprotKB (release 09-2019) containing 20369 proteins (Tyanova et al., 2016). A maximum of 5 modifications and 2 miscleavages was set using fixed carbamidomethyl modification, and the variable modifications oxidized methionine and protein N-terminal acetylation. The protein and peptide false discovery rates were set to < 0.01 and conducted with match between runs enabled. Further analysis was performed using artMS version 1.12.0 building on MSstats (Choi et al., 2014; Jimenez-Morales et al., 2019). MSstats imputation was done using accelerated failure time modeling, and the samples were median normalized after imputation.

FGFR qPCR quantification

MCF-7 cells were plated in triplicates. Subsequently, the samples were lysed and prepared for qPCR analysis using the protocol adapted from (Korsten et al., 2022). In short, samples were lysed and isolated using the vendor's instructions of NucleoSpin RNA plus (Macherey-Nagel) with the addition of a DNase removal step using RNase-Free Dnase (Qiagen). Next, 500 ng of RNA was used to obtain cDNA using the vendor's instructions of AH iScript (Bio-Rad). The qPCR was performed at 95C for 10min, followed by (95C for 30 sec, 55C for 30 sec, and 72C for 30sec), a total of 40 times. Normalization was performed using Beta-actin and Glyceraldehyde-3-phosphate dehydrogenase following (Taylor et al., 2019). The primers used are listed in supplementary table 1.

RAP1 activation assay

RAP1 activity was determined following the supplier's instructions (Merck, Cat# 17-321). In short, MCF-7 cells were plated in 15cm plates and incubated for 60 minutes with FGF2, FGF3, FGF4, FGF10, FGF19, or without FGF and lysed using the provided lysis buffer. After, equal amounts of protein were used for the RAP1 pulldown, including one positive control consisting of MCF-7 cell lysates incubated with GTPγS. Subsequently, a western blot was conducted using the provided RAP1 antibodies. Linear adjustments were performed using Fiji (Schindelin et al., 2012).

Results

Dynamic kinase activity quantification

Here we performed (phospho)proteomics experiments to elucidate the specific effect of different FGF ligands on FGFR activation and downstream signaling. Thereby we focused on FGFR signaling in breast cancer cells induced by either FGF2, FGF3, FGF4, FGF10, or FGF19. To understand signaling, we quantified temporal system-wide kinase activity using a dedicated selected reaction monitoring (SRM) assay targeting the activation loops of a widespread panel of kinases (**Figure 1A**). To increase kinome coverage of the kinases involved in the FGFR signaling pathway, nearly 200 phosphopeptides spanning 50 kinases were included in the assay earlier developed by Schmidlin et al. (2019), resulting in an assay comprising 484 phosphopeptides on 197 kinases (**Table S1**) (Schmidlin et al., 2019).

To select an appropriate cell line, this SRM assay was initially used to monitor the system-wide kinome activity response of a set of breast cancer cell lines, namely MCF-7, BT-474, and EFM-192a cells, upon FGF2 and FGF4 stimulation as these bind the majority of FGFR spliceoforms. From these data, we concluded that MCF-7 cells especially displayed a broad kinome response after stimulation (**Figure S1**). We reasoned this would be explained by FGFR expression, however, surprisingly, qPCR quantification of FGFR expression in the panel of tested cells showed that the MCF-7 cells exhibited an overall low expression of FGFRs (**Figure 1B** and **Figure S2**). This highlights that FGFR expression alone does not solely determine the extent of downstream signaling. Due to the observed broad kinome response, we did proceed with the MCF-7 cells, which were incubated with either FGF2, FGF3, FGF4, FGF10, or FGF19, and the cofactor heparin for 0, 5, 15, 30, and 60 minutes (Eswarakumar et al., 2005; Wolf et al., 2008). Using the kinase activation loop SRM assays, we quantified kinase activity profiles of 46 phosphorylated sites spanning 44 kinases (**Table S2**). Of these, 35 kinases displayed significant regulation over time (ANOVA $p < 0.05$) upon stimulation with at least one of the 5 tested FGF ligands. Each of the tested ligands resulted in differential regulation of kinases across most kinase families (**Figure 1C**) that were, as expected, primarily members of the MAPK/ERK, PI3K, and/or PLCγ pathways (**Figure 1D/E**) (Ornitz & Itoh, 2015, 2022).

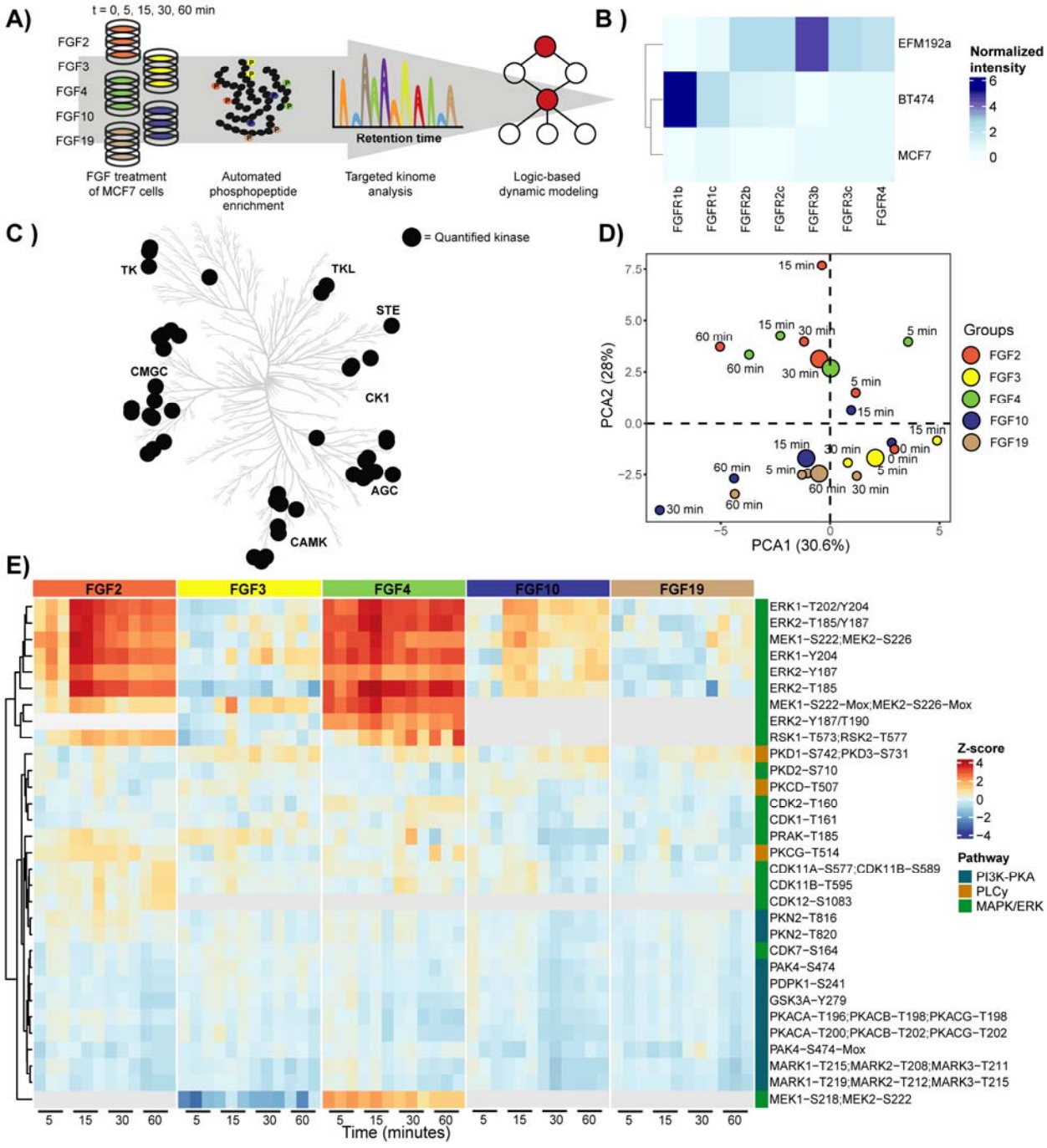

Figure 1. Stimulation with FGF2, FGF3, FGF4, FGF10, or FGF19 results in differential kinome regulation. A) Schematic overview of the experimental approach, whereby a targeted kinase activation loop SRM assay was used to monitor system-wide kinase activity upon treatment of MCF-7 cells with distinct FGF ligands. **B)** qPCR experiments were performed to monitor FGFR expression on three different cell lines. FGFR expression was normalized to Beta-actin and Glyceraldehyde-3-phosphate

dehydrogenase. **C)** Kinome tree with kinases significantly regulated by at least one of the tested FGF ligands represented by black dots (ANOVA $p < 0.05$, triplicate measurements). **D)** Principle Component Analysis (PCA) of the kinase activity data at different time points and with the different tested FGFs. Mean values were used for the independent triplicate measurements. **E)** Heatmap through unsupervised hierarchical clustering of all significantly (ANOVA $p < 0.05$) regulated phosphorylated peptides over all time points and FGFs (with each experiment performed in triplicate). Not identified phosphorylated peptides are represented in grey.

Fine-tuned activation of the MAPK/ERK signaling pathway

As the MAPK/ERK pathway is known to be involved in FGF signaling, we first compared the kinase activity profiles acquired with the SRM assays of kinases involved in this pathway. FGF-stimulated MAPK/ERK activation is commonly regarded to be directed via the RAS-RAF-MEK-ERK signaling cascade (Azami et al., 2017; Bockorny et al., 2018; Cho et al., 2009; Kunath et al., 2007; Lovicu & McAvoy, 2001; Shalaby et al., 2009; Tomita et al., 2021). In MCF-7 cells, only FGF2, FGF4, and FGF10 treatments significantly activated several of the kinases in the MAPK/ERK pathway (**Figure 2A**).

Investigating the kinases involved in the MAPK/ERK pathway after either FGF2, FGF4, or FGF10 treatment, showed rapid and high regulation of especially the main signaling hub of the MAPK/ERK pathway, namely MEK (MEK1 and MEK2) and ERK (ERK1 and ERK2) (**Figure 2B**) (Lavoie et al., 2020). FGF2 and FGF4 treatment resulted in an >10-fold increase of MEK and ERK activating phosphorylation and FGF10 an >2-fold increase. Notably, MEK and ERK activation was about 10-fold higher compared to the other kinases in the MAPK/ERK pathway, supporting their central role as signaling hub (**Figure 2B**). MEK and ERK dynamics per FGF treatment showed high correlation, displaying direct regulation of ERK as the target of MEK. However, MEK and ERK signaling dynamics showed a lower correlation between different FGF stimulations, also in the case of strong activation via FGF2 and FGF4. FGF4 treatment resulted in fast activation peaking at 15 min and showing an additional increase after the 30-minute time-point. FGF2 treatment on the other hand showed slightly slower activation with also the maximum at 15 minutes that plateaus from 30 minutes onwards (**Figure 2B**). This suggests differential MAPK/ERK pathway regulation.

Even though FGF2, FGF4, and FGF10 all activated MEK and ERK, all ligands resulted in unique downstream activation, which could either be the result of different activation mechanisms and feedback loops or due to different activation dynamics of the same pathway (Aoki et al., 2013; Raina et al., 2022). After FGF2 and FGF4 treatment, but not FGF10, MEK and ERK dynamics highly correlated with RSK1 and RSK2 dynamics, which are regulators of cell proliferation and cell survival (**Figure 2B**) (Anjum & Blenis, 2008; Houles & Roux, 2018; Romeo et al., 2012). FGF2 incubation resulted in the activation of CDK12 and a transient 1.5-fold increase in activating phosphorylation of PRAK, of which the role in the context of FGF has remained elusive (Maher, 1999; New, 1998). FGF4 incubation resulted in the activation of CDK1 and CDK2. Interestingly, CDK activation dynamics are relatively modest, with a maximum increase in activating phosphorylation of 60% (**Figure 2B**). Uniquely, FGF10 treatment did not activate kinases downstream of ERK but inactivated CDK2, CDK7, CDK11a, CDK11b, and PRAK. Inactivation of these kinases occurred concurrently after 30 minutes, which may originate from a negative feedback loop (Kuo et al., 2014). FGF10 may initiate this feedback loop by recycling its receptor FGFR2b to the cell membrane, or FGFR2b intracellular transport may expose the receptor to the substrates responsible for the feedback loop (Smith et al., 2021). Notably, only FGF10 showed sustained PRAK inactivation, which has been associated with decreased tumor progression (P. Sun et al., 2007; Y. Wang et al., 2021).

FGF3 and FGF19 have been described to activate the MAPK/ERK pathway in a subset of cell lines through FGFR4 activation (Desnoyers et al., 2008; Shi et al., 2009; Shinya et al., 2001; Teng et al., 2018, p. 201). In contrast, in our dataset, we did not observe any activation of the MAPK/ERK pathway after FGF3 and FGF19 stimulations, although, in our proteome profiles of MCF-7 cells after 24 hours of incubation with different FGFs, we did clearly identify the FGFR4 receptor.

In the context of FGF stimulation, MAPK/ERK pathway activation is considered to drive cell growth and increase tumor progression (Koledova et al., 2019; Lovicu & McAvoy, 2001; Y. Sun et al., 2017). To verify whether cell growth was indeed induced in our experimental conditions, we monitored cell growth after FGF stimulations using an IncuCyte ZOOM™. Only after stimulation with FGF2 and FGF4 we temporarily observed significantly increased cell growth (two-tailed t-test, $p < 0.05$) (**Figure 2C**). This finding was in line with the high MAPK/ERK

369 pathway activation quantified in FGF2 and FGF4-stimulated cells. FGF10 stimulation did not
370 substantially increase cell growth even though the MAPK/ERK pathway was activated. This
371 suggests that a signaling threshold must be reached to activate proliferation or that alternative
372 signaling is required for cell growth. Notably, adding heparin significantly increased the
373 proliferation rate of FGF2 and FGF4-treated MCF-7 cells, while only adding heparin did not
374 increase cell proliferation (**Figure 2C**).

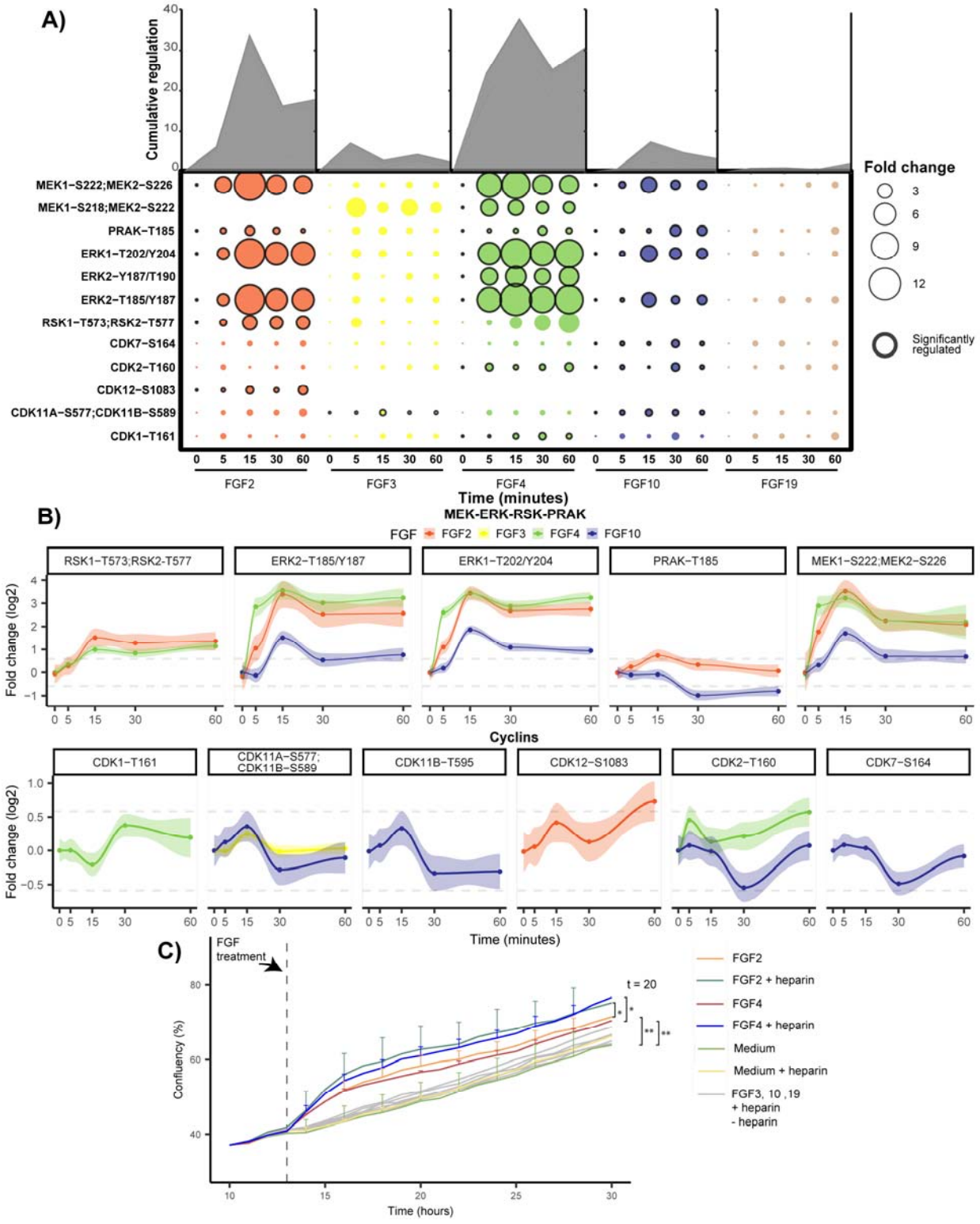

Figure 2. Regulation of kinases and cyclins implicated in the MAPK/ERK pathway. A) Measured phosphorylated peptides involved in the MAPK/ERK pathway that show significant regulation (ANOVA $p < 0.05$, independent triplicate measurements) following

incubation with at least one of the tested FGFs. Black-edged circles represent significant phosphosites. The area of the circle represents cumulative regulation in fold change of the measured phosphopeptides measured in triplicate over 5 subsequent time points. The dynamic phosphorylation of the sites is color-coded by the FGF ligand used, and only plots are depicted when the ligand changed the phosphorylation at that site significantly. Grey lines represent a 1.5 fold-change, and 90% confidence intervals are presented per phosphopeptide. **C)** Influence of incubation with the FGF ligand and heparin on cellular growth. Growth curves of MCF-7 cells, incubated with 50ng/mL of each of the tested FGF ligands with or without 5µg/mL of heparin. The confluency percentage was taken as a readout to analyze cell growth and plotted (data was acquired in triplicate showing the standard deviations per time point and ligand used).

Consistent down-regulation of the PI3K and PKA pathway

Next, we examined the PI3K and PKA pathways. In our analysis, incubation with each of the tested FGFs, except FGF3, resulted in the significant inactivation of the PI3K and PKA pathways (**Figure 3A**). The PKA pathway is not commonly described to be regulated by FGFs. However, we quantified the change in phosphorylation of the upstream regulator PDPK1, which directly regulates PKA activity by phosphorylating Thr-197 (Cauthron et al., 1998). All measured kinases involved in the PKA pathway highly correlated with PDPK1 dynamics for all FGF stimulations in our dataset, revealing possible crosstalk between the PI3K and the PKA pathway.

All tested FGFs, except for FGF3, resulted in similar inactivation of PDPK1 and the PKA pathway kinases PKA, GSK3A, and MARK kinases (**Figure 3B**). Inactivation was consistent but modest. The most significant decrease was a 2-fold decrease on two phosphorylated sites in the activation loop of MARK1, MARK2, and MARK3, respectively (**Figure S3**). Notably, no relation has been described between MARK kinases and FGF signaling up to this day. MARK kinases control cell polarity by regulating microtubules, and reduced MARK kinase activity has been linked to EMT, which is in line with the EMT-inducing effects of FGFs (Drewes et al., 1997; Sonntag et al., 2017).

Besides the similar PI3K and PKA pathway regulation by FGF2, FGF4, FGF10, and FGF19, solely FGF10 stimulation led to a decrease in phosphorylation of the downstream kinases PAK4, DYRK1A, DYRK1B, and PKN (**Figure 2B**). This reveals broad FGF10-induced negative regulatory mechanisms. Notably, the inhibited PAK4, which plays a role in cell adhesion, can be

regulated via ERK and the PI3K pathway (Qu et al., 2001; Ramos-Alvarez & Jensen, 2018; Thillai et al., 2017; Won et al., 2019). The observed kinase activity dynamics of PAK4 strongly correlated with the rest of the PI3K pathway while opposing the MAPK/ERK pathway activity dynamics. This observation suggests that PAK4 is linked to the PI3K pathway, not the MAPK/ERK pathway.

FGF2, FGF4, FGF10, and FGF19 have all been described to induce EMT, which is thought to be partially regulated via the regulation of the PI3K pathway and is regarded as a key process in regulating tumor metastasis (Katoh & Katoh, 2006; B. P. Zhou et al., 2004). This agrees with the targeted kinome data that revealed PI3K pathway inactivation for these FGFs. To investigate whether the tested FGFs induced EMT, we next performed a wound-healing assay that assays cell migration capabilities, which is a key process in EMT (Grada et al., 2017; Yan et al., 2010). These assays revealed that, only FGF2 and FGF4 showed a significant increase in wound-healing capacity of 15 and 5% compared to unstimulated MCF-7 cells, respectively (**Figure 3C**). Interestingly, with the addition of heparin, this dampened to 10% for FGF2 and increased to 40% for FGF4, revealing a modest role for heparin in regulating EMT. To find further support for FGF-induced EMT, we extracted proteins from the EMTome database associated with EMT, specifically focusing on proteins that directly trigger EMT or are key markers for EMT (Vasaikar et al., 2021). In their proteomic profiles (**Table S3**), FGF2 and FGF4 stimulations showed an identical profile of 15 EMT-associated proteins significantly regulated after 24 hours (**Figure 3D**), supporting an EMT-like phenotype downstream of FGF2 and FGF4. FGF10 stimulation resulted in less pronounced expression changes in 7 of the 15 observed EMT proteins, in part confirming the role of FGF10 in inducing EMT, whereas FGF3 and FGF19 showed no significant expression changes in EMT-related proteins (Brabletz et al., 2018). This is further supported by GSEA analysis of the hallmarks of EMT as provided by MSigDB, which in our proteome data are only significantly upregulated after FGF2 and FGF4 treatment (**Figure S4**) (Subramanian et al., 2005). Altogether, these findings show FGF2, FGF4, FGF10, FGF19 all inactivated the PI3K pathway. However, only FGF2 and FGF4-treatment resulted in increased wound healing capacities and an EMT-like phenotype on proteome level, FGF10 treatment only resulted in a more EMT-like phenotype on proteome level, and FGF19 did not show either. Besides PI3K inactivation, further mechanisms must thus be regulated to induce EMT.

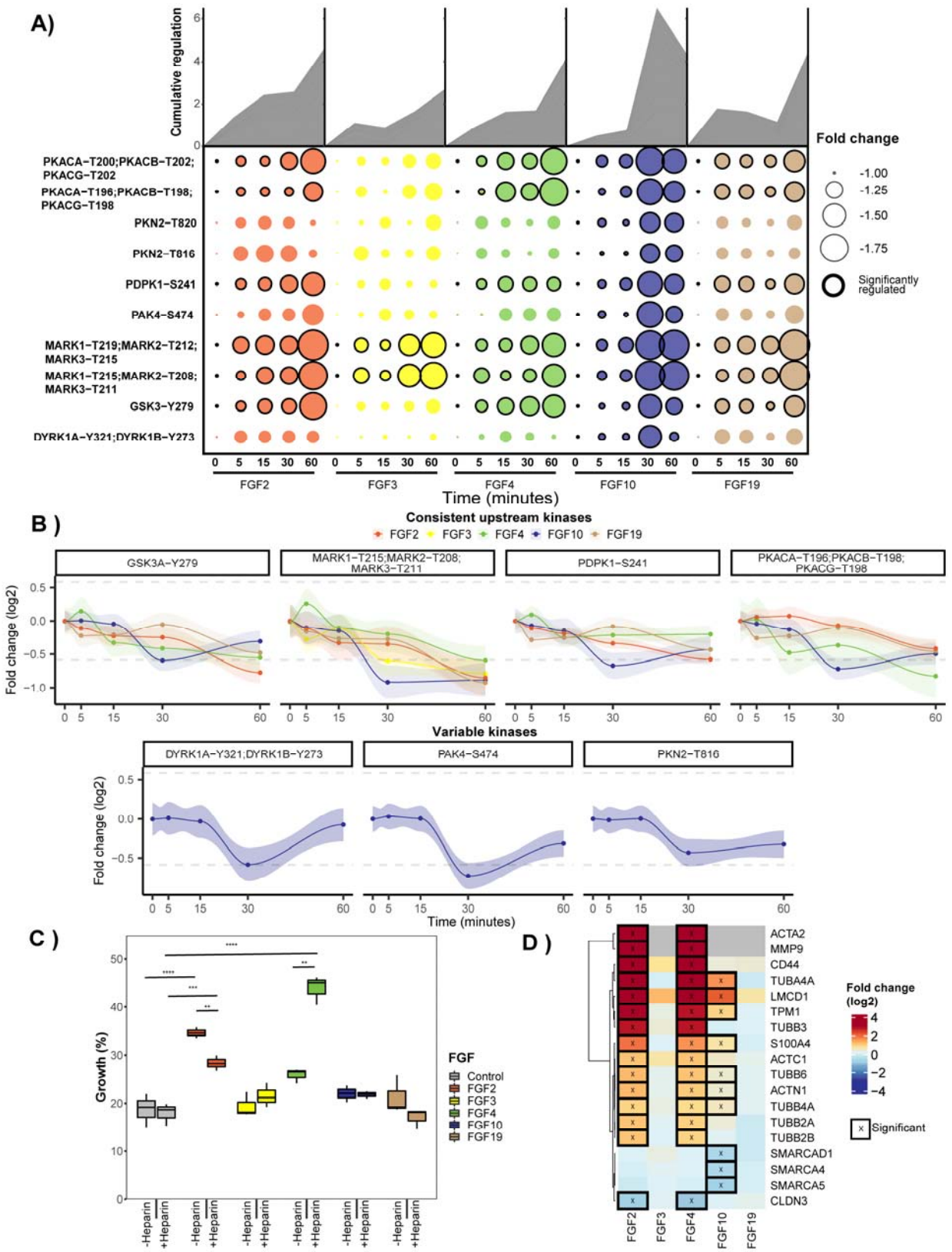

441

Figure 3. Regulation of kinases implicated in the PKA and PI3K pathways A) All significantly regulated phosphopeptides of the PI3K pathway are represented as the mean across triplicates ($p < 0.05$ ANOVA). Cumulative absolute regulation in fold change is represented in the area plot to show overall pathway regulation. **B)** Regulation of significant (ANOVA $p < 0.05$) changing phosphopeptides are plotted from the PI3K pathway. Grey lines represent a 1.5 fold-change and 90% confidence intervals are presented per phosphopeptide. **C)** MCF-7 cells were subjected to a scratch wound assay, and after 24 hours percentage closure of the scratch was measured. The boxplots represent triplicate measurements of FGF-stimulated cells with or without 5 µg/µL heparin. A two-sided t-test was used to validate the significance. **D)** Proteins associated with EMT were extracted from the shotgun dataset. Significantly regulated proteins are displayed using an asterisk (FDR < 0.05).

Undistinguished PLCγ signaling along the FGF-FGFR axis

Next, we explored the measured activity profiles of the kinases within the PLCγ pathway. The PLCγ pathway is relatively understudied in the context of FGFR stimulation and regulates specialized functions (Kim et al., 2003; Lima et al., 2009; Mohammadi et al., 1991; Niger et al., 2010; Ranieri et al., 2020; Szybowska et al., 2021). In our current study, PKD1, PKD2, PKD3, PKCδ, and PKCγ showed significant regulation when incubated with at least one of the tested FGFs (**Figure S5**). Kinase activation dynamics were non-linear, hinting at the presence of multiple feedback loops (Kuo et al., 2014). Moreover, kinases in the PLCγ pathway showed a relatively low correlation in their activation dynamics, and all tested FGFs showed distinct kinase regulation (**Figure S5**).

Indeed, only FGF2 transiently activated PKCα/β/γ by activating phosphorylation Thr-514, yet no other PLCγ pathway kinases were regulated (Kelher et al., 2017). FGF4, FGF10, and FGF19 all activated PKD1 and PKD3, whereas FGF4 and FGF10 also showed the inactivation of PKCδ and PKD2 or only PKCδ, respectively.

Distinct FGF ligands induce distinct and diverse temporal dynamics in phospho-signaling

Not only does FGF specificity to the various FGFRs determine the biological outcome, but also the affinity for the various FGFRs is crucial. In RTKs biology, it is known that ligands with high affinity to the receptor can lead to fast, transient activation, while lower affinity ligands, binding to the same receptor, lead to a slower sustained activation, resulting in a different biological

outcome (Huang et al., 2017; Kiyatkin et al., 2020). To evaluate whether each FGF differentially regulated signaling dynamics, OmniPath was used to construct biological networks in which kinases are ordered based on the initial time point when regulation was observed (**Figure 5**) (Türei et al., 2016).

Indeed, in our data, each of the tested FGFs did lead to distinct timing of initial pathway regulation. FGF2 induced a fast initial activation within 5 minutes of all measured pathways. This is expected as FGF2 binds to most FGFRs with high affinity (Ornitz et al., 1996). Although FGF4 binds the same FGFR subset as FGF2, except for FGFR1b, it does so with different affinity. As a potential consequence, and in contrast to FGF2, FGF4 stimulation inactivated the PI3K and PKA pathways in our experiments only after 15 minutes (**Figure 5**). FGF10 stimulation activated the MAPK/ERK pathway within 5 minutes, similar to FGF2 and FGF4. However, this was followed by a strong downregulation after 30 minutes of more downstream targets. Last, FGF3 and FGF19 resulted in relatively slow (and modest) activation only 30 minutes after stimulation (**Figure 5**).

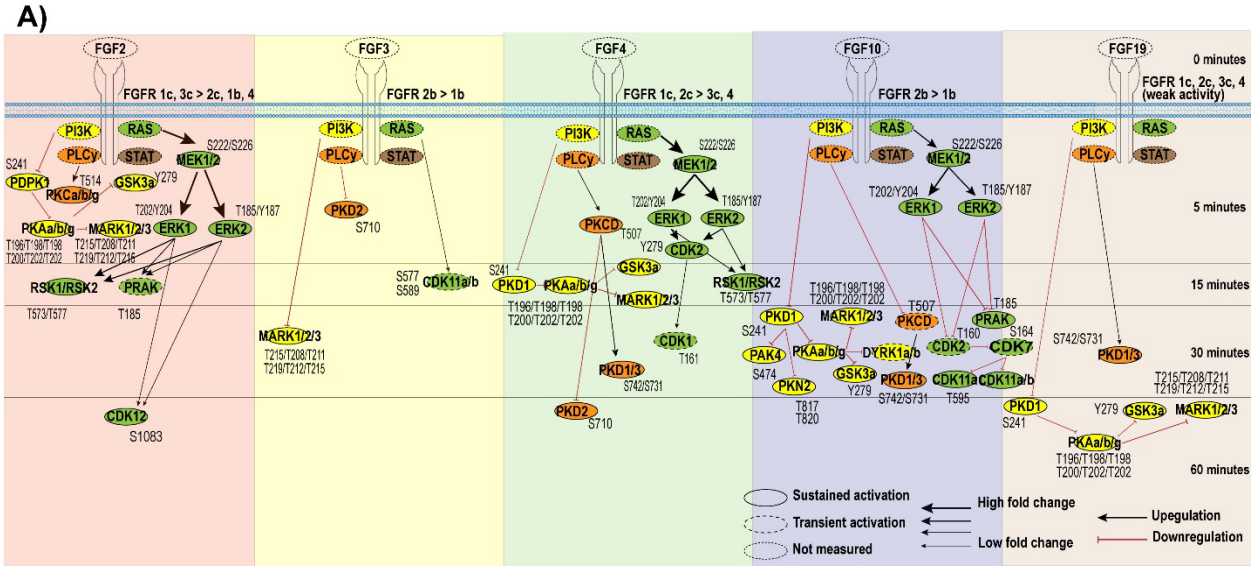

Figure 5. Temporal kinome dynamics following FGF treatment. A) MCF-7 cells were treated with either FGF2, FGF3, FGF4, FGF10, or FGF19, together with heparin. The resulting temporal kinome dynamics were quantified using the targeted activation loop assay and normalized to the t=0 time point. The presented kinome signaling dynamics are separated per FGF used for stimulation, and kinases are ordered based on significant initial activation (ANOVA + Tukey's

range test, $p < 0.05$, biological triplicates). Black and red arrows indicate whether measured kinase activity increased or decreased over time, respectively. The fold change compared to the t=0 time point is represented by the thickness of the arrows.

Logic-based dynamic modeling validates the known FGF pathways but also identifies putative new players

Pathway models such as in Figure 5 are based on existing knowledge and are thus inherently biased towards well-characterized pathways. Therefore, validation of the biological model is needed to identify either missing or inaccurate connections between kinases or missing signaling nodes. To verify our biological model, predict signaling dynamics between kinases, and find possible gaps, we used a dynamic mechanistic model based on logic-based ordinary differential equations (Morris et al., 2010). First, a prior knowledge network (PKN) was built using information available via OmniPath using only kinases quantified in all FGF stimulations (**Figure 5**) (Türei et al., 2016). Next, the logistic-based ordinal differentiations were calculated using the quantitative longitudinal kinase activity data of all FGF stimulations together. For each node, a speed factor (τ) was calculated to represent the responsiveness of a kinase's activation to upstream kinases activation (Wittmann et al., 2009). Low values indicate a slow transfer of activation from kinases' upstream activators. For each node, also an edge-specific transmission parameter (k) was calculated, which represents the quantitative signal that is transferred between kinases (Wittmann et al., 2009). High values of the non-linear k parameters indicate that relatively little quantitative signal is transferred via the edge. To evaluate the quality of the predicted τ and k values, Pearson's r and the RMSE of all the quantitative kinome values in the model were assessed and compared to the RMSE between biological replicates (**Figure 6A** and **B**). The RMSE of the model (0.18) is almost as low as the RMSE observed between the biological replicates (0.1). The model thus successfully predicts most of the kinase activity, with a small error likely due to unknown entries in the PKN.

To explore these unknowns in the PKN, the RMSE of individual phosphopeptides was evaluated (**Figure 6C**). High RMSE suggests that the model is insufficient to predict a kinase activation state, which results from missing or erroneous connections between nodes in the network. Therefore, a high predictive error can be used to find novel biological connections or nodes. The model showed no highly contradictive prediction errors for single kinases (RMSE error > 0.5),

which occurs when activation of one kinase leads to activation of the next kinase, but inactivation is measured. However, some kinases showed errors that were higher than the biological variance.

Kinases with a relatively high error are part of the PLCγ and MAPK/ERK pathways. Error in kinases regulated by the PLCγ pathway is expected due to the low pathway coverage (**Figure 5**). Surprising, however, is the substantial error in MEK activity prediction after FGF2 stimulation (**Figure 6C**). The model failed to predict the fast activation of MEK and ERK, and did not incorporate the oscillatory patterns typical for feedback loops (**Figure 6D**). Further, following MEK-ERK signaling downstream, all measured CDKs, including CDK1, CDK2, CDK7, CDK11a, and CDK11b, show a relatively high predictive error. This suggests differential MEK-ERK signaling to their downstream effectors. We, therefore, hypothesized that the error in MEK-ERK-CDK signaling is indicative of unknown links between kinases or missing nodes in the current model. We will focus on this more in the next section.

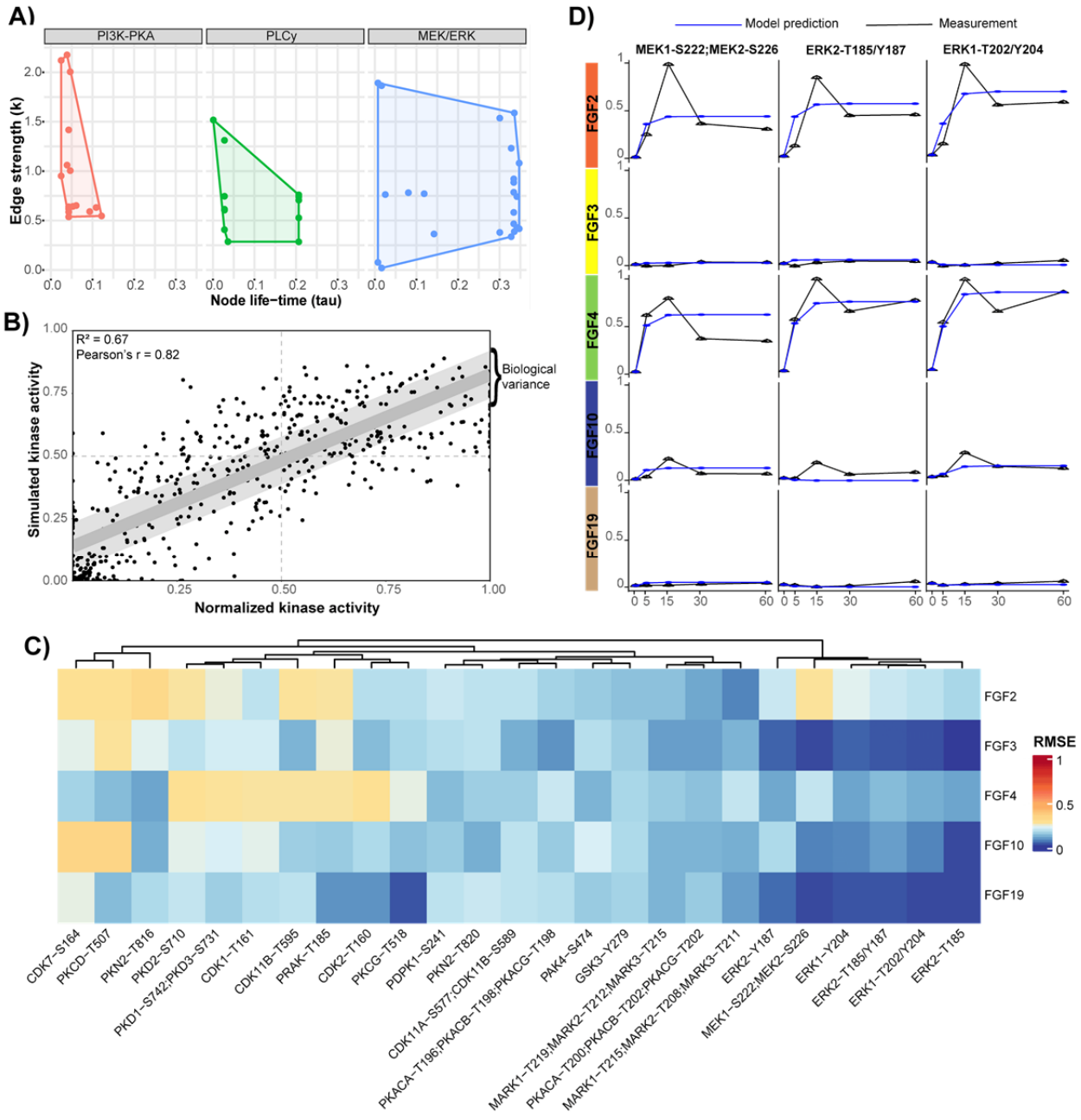

536

537 **Figure 6. Logic-based dynamic modeling reveals unknowns in FGF-induced signaling.**
538 **A)** Logic-based dynamic modeling was used to predict a speed factor (τ) and a
539 transmission parameter (k) for the kinases across the PI3K, PKA, PLCγ, and MAPK/ERK
540 pathways. These represent the signal transduction speed and the quantitative signal
541 transferred between kinases, respectively. **B)** The root mean squared error (RMSE) of the
542 predicted values by logic-based dynamic modeling and the measured values by the
543 targeted kinome loops assay. The values were normalized using the 99% interquartile
544 range. The light grey area represents the biological variation in the measurements. The

dots represented are the mean values of the replicates and all time points. **C)** Mean RMSE values for the measured vs. predicted kinase activity values. The modeling was performed using identical networks, meaning downstream kinase-kinase relations constitute the same predictive k and tau values. Therefore, predictive downstream errors may indicate differential regulation between FGFs. **D)** Line plots of the measured and predicted kinase activity using the function with the lowest error across all FGF stimulations. Before the logic-based dynamic modeling, the average of the quantified kinome values was taken (biological triplicates) and normalized using the 99% interquartile range. The blue line represents the model prediction, and the black line represents the quantified kinase activity using the targeted kinome assay.

Modeling guided analysis unveils differential FGF signaling

With the aim to explain the predictive modeling errors for MEK, ERK, and CDKs, we expanded the model using manually curated literature mining, shotgun phosphoproteomics analysis of FGF-stimulated MCF-7 cells (**Table S4**), and our targeted kinome data. Significantly regulated proteins were used to construct a more refined pathway (**Figure 7A**) (Gotoh, 2008; Hadari et al., 1998; Yang et al., 2006).

A potential missing link came from the phosphoproteomics data that suggested a RAP1 activation signature exclusively for FGF2. RAP1 is an alternative activator of MEK-ERK, whose activators include EPAC2 and SRC, and its main negative regulator is RAP1gap (**Figure 7A**) (Looi et al., 2020; Schmitt & Stork, 2002; Stokman et al., 2014). Uniquely, FGF2 treatment abolished the signal of Tyr-284 and Thr-301 phosphorylation of EPAC2, which is important for EPAC2 membrane localization. Moreover, FGF2 treatment increased activating phosphorylation Ser-17 of SRC about 4-fold and resulted in a 1.6-fold increase in regulating phosphorylation Ser-484 on RAP1gap (Daumke et al., 2004; de Rooij et al., 2000; Fukuyama et al., 2005, 2006; Rehmann et al., 2003, 2006). These phosphorylations highlight possible RAP1 activation. Therefore, we conducted a RAP1 activity assay. However, this RAP1 activation assay showed no significant RAP1 activation in all tested ligands (**Figure S6**). From these data, we concluded that although pathways commonly involved in RAP1 activation were regulated, RAP1 was not activated and thus was not the cause of differential MEK-ERK dynamics.

Next, we compared FGF2 and FGF4-induced signaling along a more detailed RAS-RAF-MEK-ERK signaling axis (**Figure 7A** and **B**). FGF2 and FGF4 treatment resulted in fine-tuned and

576 distinct regulation along this signaling axis, especially of the RAF family members (ARAF,
577 BRAF, RAF1) that coordinate MEK-ERK activation (Maurer et al., 2011). Solely FGF2
578 treatment enabled BRAF activity by abolishing the signal of the inhibitory ERK target site Ser-
579 151 on BRAF (**Figure 7B**) (Marquette et al., 2011). Moreover, FGF2 treatment resulted in
580 reduced activity of ARAF following significant downregulation of Ser-582 phosphorylation,
581 which is needed for 14-3-3 binding to increase the activity of ARAF (Baljuls et al., 2008). FGF2
582 also resulted in a reduced active state of RAF1 implied by an 8-fold lower signal of Ser-621
583 phosphorylation, necessary for 14-3-3 activation, and by the negative feedback phosphorylation
584 of Ser-642 by ERK on RAF1 (**Figure 7B**) (Dhillon et al., 2009; Zang et al., 2008) (Dougherty et
585 al., 2005). Contrarily, FGF4 stimulation showed an activating signature for ARAF, indicated by
586 the phosphorylation of the regulatory site Ser-186 on ARAF (Stuart et al., 2015). Further, FGF4
587 stimulation resulted in inhibitory phosphorylation on BRAF and RAF1, with a twofold increase
588 in Ser-151 phosphorylation on BRAF, and a strong increase in Ser-642 phosphorylation on
589 RAF1, which was absent in the control (**Figure 7B**). In conclusion, the RAF family members
590 showed differential regulation as FGF2 treatment indicated BRAF-driven activation, while FGF4
591 treatment indicated ARAF-driven activation.

592 To further validate these signaling differences, we again applied logic-based dynamic modeling
593 using the data from the targeted kinome assay. In the updated model, FGF2 signaling was
594 directed via BRAF and FGF4 via ARAF. Moreover, to model the negative feedback loops, one
595 negative feedback loop between ERK and the FGF activation of ARAF and BRAF was added, as
596 well as a negative feedback loop from ERK to RKIP and from RKIP to ARAF and BRAF
597 activation of MEK (Shin et al., 2009). The updated pathway showed improved modeling
598 accuracy (**Figure 7C**). Especially the FGF2 signaling prediction now has high accuracy that
599 follows the measured feedback loops, giving confidence to the predicted biological pathway.
600 Prediction of FGF4 signaling dynamics was also improved over the initial model, with more
601 accurately modeled activation dynamics, however, is not optimal yet (**Figure 7C**). Indeed, the
602 updated model supports the two different modes of ERK activation downstream of FGF2 and
603 FGF4, yet, alternative regulators need to be identified to fully explain FGF signaling dynamics.

604 Following ERK activation further downstream, we set out to use the shotgun phosphoproteomics
605 data to confirm predictive errors for the CDKs and validate differential regulation downstream of

606 ERK. Cumulatively, 17 different phosphorylated sites on proteins that regulate the cell cycle
607 were quantified, including CDKs, cyclins that regulate CDK activity, and RB1, which are all
608 central to cell cycle progression (**Figure 7D**) (Loog & Morgan, 2005; Valverde et al., 2022).
609 FGF3, FGF10, and FGF19 showed little CDK regulation in our model, in line with the targeted
610 kinome data and the modeling results. FGF2 and FGF4 showed distinct activation patterns of
611 CDKs (**Figure 7D**), agreeing with the targeted kinome data and the modeling error. These
612 distinct activation patterns confirm the predictive error of the dynamic model and show that
613 FGF2 and FGF4 regulate cell cycle progression differently.

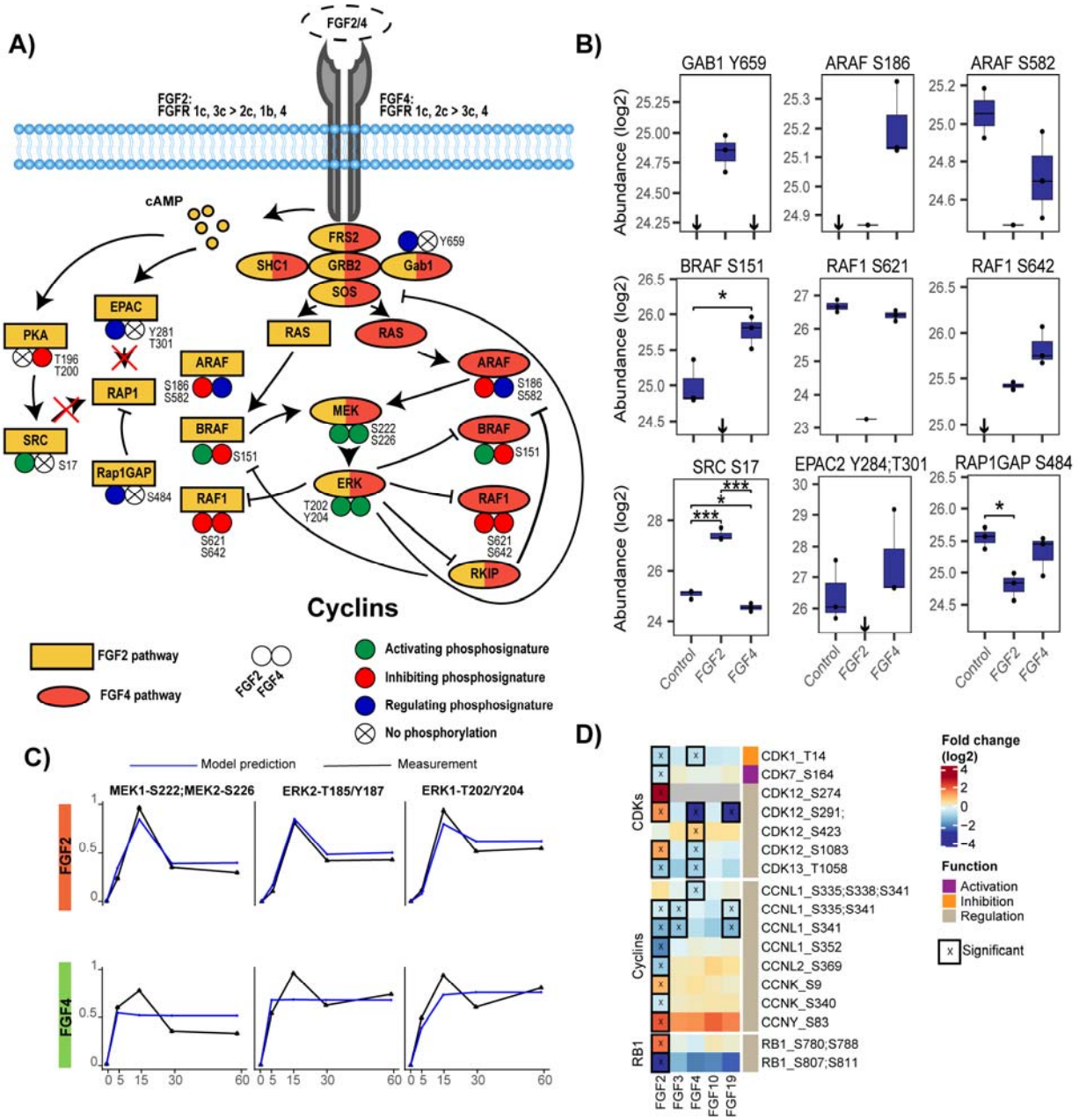

614

615 **Figure 7. Regulation of RAF family kinases modulates ERK signaling. A)** Mapping of
616 phosphorylations of proteins involved in ERK activation shows tight regulation of the
617 RAF kinase family members. The regulation does occur in the RAP1 activation pathway of
618 ERK, yet no RAP1 activation was measured, suggesting this does not contribute to ERK
619 activation. **B)** Quantified peptide abundances corresponding to figure 7A. Significance is
620 depicted using * ($p < 0.05$) or *** ($p < 0.001$) using a two-sided t-test (biological
621 triplicates). If all values are below the detection limit, this is shown using a ↓.
622 Abundances are acquired using shotgun phosphoproteomics after 60-minute stimulation

with the different FGFs. **C)** Line plots of the measured kinase activity and the predicted kinase activity using the function with the lowest error across all FGF stimulations. The PKN used is the updated biological pathways, also presented in figure 7A. The average of biological triplicates was taken and normalized using the 99% interquartile range. Model predictions are shown in blue, and quantified kinase activity is shown in black. **D)** Phosphorylation of cell cycle regulating proteins from the phosphoproteomics data. Significant regulated sites are displayed (two-sided t-test, $p < 0.05$, biological triplicates). Scores represent log2 fold changes.

Discussion

By investigating the FGF-induced dynamic kinome regulation using a targeted kinome assay, we quantified and compared the signaling responses of FGF2, FGF3, FGF4, FGF10, and FGF19. All FGF stimulations resulted in a unique biological response in MCF-7 cells, with FGF2 and FGF4 having the broadest kinome response, FGF10 having a moderate response, and FGF3 and FGF19 showing a modest response. We find complex activation mechanisms that initiate FGF signaling as biological responses upon FGF stimulation vary between cell lines, do not correlate with FGFR expression level and are influenced by heparin.

Looking at the FGFs in a breast cancer context, FGF-stimulated cells activate biological pathways that can contribute to the hallmarks of cancer (Hanahan & Weinberg, 2011; Xie et al., 2020). The MAPK/ERK pathway is thought to drive cell proliferation, and the PI3K pathway is believed to regulate EMT (Kunath et al., 2007). However, we find that simply activating these pathways does not per se lead to cell proliferation or EMT, respectively. Importantly, this irregularity between kinome or pathway activation and predicted biological outcome emphasizes the complexity of these processes and their incomplete understanding. FGF2 and FGF4 increased cell proliferation and EMT in MCF-7 cells. However, FGF3, FGF10, and FGF19 are reported to regulate cell proliferation and EMT but were not able to regulate these processes in our system. Additional signaling factors may be needed to sensitize or co-stimulate the cells for a more pronounced biological response (Desnoyers et al., 2008; W. Wang et al., 2015; Watson & Francavilla, 2018).

The quantification of dynamic kinase responses instead of single time points is highly advantageous for understanding FGF-stimulated signaling because these dynamics expose

unknown signaling routes and improve the reliability of the predicted signaling network. Often biological networks are deduced from literature without proper validation. For this purpose, logic-based dynamic modeling provides a suitable solution. Logic-based dynamic modeling of the FGF stimulations resulted in an overall low network error implying feasible network predictions. Mainly the PLCγ pathway showed higher predictive errors due to a higher sparsity of the network, partly due to limited insights into PLCγ signaling in the FGF context. This highlights the importance of further studying PLCγ signaling to understand its functions in FGF signaling (Brewer et al., 2016).

The dynamic modeling highlighted differential and fine-tuned regulation of the MAPK/ERK pathway. Regulating phosphorylations of the RAF kinases indicate that FGF2 stimulation is directed via BRAF, while FGF4 stimulation is directed via ARAF. Literature on RAF kinase family regulation by FGFs is limited; however, understanding RAF regulation is essential because different RAF kinases perform different biological functions (Dumaz, 2011; Wellbrock et al., 2004). Moreover, understanding RAF signaling provides targeted insights that can be exploited to successfully deploy RAF specific inhibitors in various diseases, such as cancer (Saini et al., 2013). For example, Metzner et al., show that FGF-driven melanoma is, in some cases, sensitive to the BRAF inhibitor RG7204 (Metzner et al., 2011).

To conclude, this study highlights the differential signaling of FGFs and adopts existing logic-based dynamic modeling techniques to direct, strengthen, and increase the discovered biological knowledge.

Acknowledgments

We thank Mara Diks and Suzan Thijssen (Utrecht University) for their guidance with the qPCR experiments. We thank Jennifer Haworth and Joseph Parsons (CF team) for providing qPCR sequences. This work has been supported by EPIC-XS, project number 823839, funded by the Horizon 2020 programme of the European Union and the NWO funded Netherlands Proteomics Centre through the National Road Map for Large-scale Infrastructures program X-Omics, Project 184.034.019. Research in CF lab is supported by the Wellcome Trust (107636/Z/15/Z and 107636/Z/15/A), the Biotechnology and Biological Sciences Research Council (BB/R015864/1), and Medical Research Council (MR/T016043/1).

Author contributions

Tim S. Veth: Conceptualization; Data curation; Formal analysis; Investigation; Resources; Software; Visualization; Writing – original draft. **Chiara Francavilla**: Conceptualization; Writing – review & editing. **Albert J.R. Heck**: Conceptualization; Funding acquisition; Resources; Writing – review & editing. **Maarten A.F.M. Altelaar**: Conceptualization; Funding acquisition; Resources; Writing – review & editing.

Declaration of interest

The authors declare that they have no conflict of interest.

Data availability

Data are available via ProteomeXchange with identifier PXD038836 :

(Username: reviewer_pxd038836@ebi.ac.uk ; Password: CCMgJt8J)

Data are available via ProteomeXchange with identifier PXD038808:

(Username: reviewer_pxd038808@ebi.ac.uk ; Password: mYXS1PfR)

Data are available via ProteomeXchange with identifier PXD039005:

(Username: panorama+reviewer164@proteinms.net; Password: AlheltWY)

The used R scripts are available at: https://github.com/TVeth/FGF_Veth_2023

References

Abolhassani, A., Riazi, G. H., Azizi, E., Amanpour, S., Muhammadnejad, S., Haddadi, M., Zekri, A., & Shirkoohi, R. (2014). FGF10: Type III Epithelial Mesenchymal Transition and Invasion in Breast Cancer Cell Lines. *Journal of Cancer*, 5(7), 537–547. https://doi.org/10.7150/jca.7797

704 Anjum, R., & Blenis, J. (2008). The RSK family of kinases: Emerging roles in cellular
705 signalling. *Nature Reviews Molecular Cell Biology*, *9*(10), 747–758.
706 https://doi.org/10.1038/nrm2509
707 Aoki, K., Kumagai, Y., Sakurai, A., Komatsu, N., Fujita, Y., Shionyu, C., & Matsuda, M.
708 (2013). Stochastic ERK Activation Induced by Noise and Cell-to-Cell Propagation
709 Regulates Cell Density-Dependent Proliferation. *Molecular Cell*, *52*(4), 529–540.
710 https://doi.org/10.1016/j.molcel.2013.09.015
711 Azami, T., Waku, T., Matsumoto, K., Jeon, H., Muratani, M., Kawashima, A., Yanagisawa, J.,
712 Manabe, I., Nagai, R., Kunath, T., Nakamura, T., Kurimoto, K., Saitou, M., Takahashi,
713 S., & Ema, M. (2017). *Klf5* maintains the balance of primitive endoderm to epiblast
714 specification during mouse embryonic development by suppression of *Fgf4*.
715 *Development*, dev.150755. https://doi.org/10.1242/dev.150755
716 Baljuls, A., Schmitz, W., Mueller, T., Zahedi, R. P., Sickmann, A., Hekman, M., & Rapp, U. R.
717 (2008). Positive Regulation of A-RAF by Phosphorylation of Isoform-specific Hinge
718 Segment and Identification of Novel Phosphorylation Sites. *Journal of Biological*
719 *Chemistry*, *283*(40), 27239–27254. https://doi.org/10.1074/jbc.M801782200
720 Bockorny, B., Rusan, M., Chen, W., Liao, R. G., Li, Y., Piccioni, F., Wang, J., Tan, L., Thorner,
721 A. R., Li, T., Zhang, Y., Miao, C., Ovesen, T., Shapiro, G. I., Kwiatkowski, D. J., Gray,
722 N. S., Meyerson, M., Hammerman, P. S., & Bass, A. J. (2018). RAS–MAPK
723 Reactivation Facilitates Acquired Resistance in *FGFR1* -Amplified Lung Cancer and
724 Underlies a Rationale for Upfront FGFR–MEK Blockade. *Molecular Cancer*
725 *Therapeutics*, *17*(7), 1526–1539. https://doi.org/10.1158/1535-7163.MCT-17-0464

726 Brabletz, T., Kalluri, R., Nieto, M. A., & Weinberg, R. A. (2018). EMT in cancer. *Nature*
727 *Reviews Cancer*, *18*(2), 128–134. https://doi.org/10.1038/nrc.2017.118
728 Brewer, J. R., Mazot, P., & Soriano, P. (2016). Genetic insights into the mechanisms of Fgf
729 signaling. *Genes & Development*, *30*(7), 751–771.
730 https://doi.org/10.1101/gad.277137.115
731 Cauthron, R. D., Carter, K. B., Liauw, S., & Steinberg, R. A. (1998). Physiological
732 Phosphorylation of Protein Kinase A at Thr-197 Is by a Protein Kinase A Kinase.
733 *Molecular and Cellular Biology*, *18*(3), 1416–1423.
734 https://doi.org/10.1128/MCB.18.3.1416
735 Chen, L. (2005). Roles of FGF signaling in skeletal development and human genetic diseases.
736 *Frontiers in Bioscience*, *10*(1–3), 1961. https://doi.org/10.2741/1671
737 Cho, K.-W., Cai, J., Kim, H.-Y., Hosoya, A., Ohshima, H., Choi, K.-Y., & Jung, H.-S. (2009).
738 ERK activation is involved in tooth development via FGF10 signaling. *Journal of*
739 *Experimental Zoology Part B: Molecular and Developmental Evolution*, *312B*(8), 901–
740 911. https://doi.org/10.1002/jez.b.21309
741 Choi, M., Chang, C.-Y., Clough, T., Broudy, D., Killeen, T., MacLean, B., & Vitek, O. (2014).
742 MSstats: An R package for statistical analysis of quantitative mass spectrometry-based
743 proteomic experiments. *Bioinformatics*, *30*(17), 2524–2526.
744 https://doi.org/10.1093/bioinformatics/btu305
745 Dailey, L., Ambrosetti, D., Mansukhani, A., & Basilico, C. (2005). Mechanisms underlying
746 differential responses to FGF signaling. *Cytokine & Growth Factor Reviews*, *16*(2), 233–
747 247. https://doi.org/10.1016/j.cytogfr.2005.01.007

748 Daumke, O., Weyand, M., Chakrabarti, P. P., Vetter, I. R., & Wittinghofer, A. (2004). The
749 GTPase-activating protein Rap1GAP uses a catalytic asparagine. *Nature*, *429*(6988),
750 197–201. https://doi.org/10.1038/nature02505
751 de Rooij, J., Rehmann, H., van Triest, M., Cool, R. H., Wittinghofer, A., & Bos, J. L. (2000).
752 Mechanism of Regulation of the Epac Family of cAMP-dependent RapGEFs. *Journal of*
753 *Biological Chemistry*, *275*(27), 20829–20836. https://doi.org/10.1074/jbc.M001113200
754 Debets, D. O., de Graaf, E. L., Liefaard, M. C., Sonke, G. S., Lips, E. H., Ressa, A., & Altelaar,
755 M. (2022). *Predicting treatment outcome using kinome activity profiling in HER2+*
756 *breast cancer biopsies* [Preprint]. Cancer Biology.
757 https://doi.org/10.1101/2022.09.23.508980
758 Desnoyers, L. R., Pai, R., Ferrando, R. E., Hötzel, K., Le, T., Ross, J., Carano, R., D'Souza, A.,
759 Qing, J., Mohtashemi, I., Ashkenazi, A., & French, D. M. (2008). Targeting FGF19
760 inhibits tumor growth in colon cancer xenograft and FGF19 transgenic hepatocellular
761 carcinoma models. *Oncogene*, *27*(1), 85–97. https://doi.org/10.1038/sj.onc.1210623
762 Dhillon, A. S., Yip, Y. Y., Grindlay, G. J., Pakay, J. L., Dangers, M., Hillmann, M., Clark, W.,
763 Pitt, A., Mischak, H., & Kolch, W. (2009). The C-terminus of Raf-1 acts as a 14-3-3-
764 dependent activation switch. *Cellular Signalling*, *21*(11), 1645–1651.
765 https://doi.org/10.1016/j.cellsig.2009.07.001
766 Dougherty, M. K., Müller, J., Ritt, D. A., Zhou, M., Zhou, X. Z., Copeland, T. D., Conrads, T.
767 P., Veenstra, T. D., Lu, K. P., & Morrison, D. K. (2005). Regulation of Raf-1 by Direct
768 Feedback Phosphorylation. *Molecular Cell*, *17*(2), 215–224.
769 https://doi.org/10.1016/j.molcel.2004.11.055

770 Drewes, G., Ebneth, A., Preuss, U., Mandelkow, E.-M., & Mandelkow, E. (1997). MARK, a
771 Novel Family of Protein Kinases That Phosphorylate Microtubule-Associated Proteins
772 and Trigger Microtubule Disruption. *Cell*, *89*(2), 297–308.
773 https://doi.org/10.1016/S0092-8674(00)80208-1
774 Dumaz, N. (2011). Mechanism of RAF isoform switching induced by oncogenic RAS in
775 melanoma. *Small GTPases*, *2*(5), 289–292. https://doi.org/10.4161/sgtp.2.5.17814
776 Eduati, F., Doldàn-Martelli, V., Klinger, B., Cokelaer, T., Sieber, A., Kogera, F., Dorel, M.,
777 Garnett, M. J., Blüthgen, N., & Saez-Rodriguez, J. (2017). Drug Resistance Mechanisms
778 in Colorectal Cancer Dissected with Cell Type–Specific Dynamic Logic Models. *Cancer*
779 *Research*, *77*(12), 3364–3375. https://doi.org/10.1158/0008-5472.CAN-17-0078
780 Egea, J. A., Henriques, D., Cokelaer, T., Villaverde, A. F., MacNamara, A., Danciu, D.-P.,
781 Banga, J. R., & Saez-Rodriguez, J. (2014). MEIGO: An open-source software suite based
782 on metaheuristics for global optimization in systems biology and bioinformatics. *BMC*
783 *Bioinformatics*, *15*(1), 136. https://doi.org/10.1186/1471-2105-15-136
784 Eswarakumar, V. P., Lax, I., & Schlessinger, J. (2005). Cellular signaling by fibroblast growth
785 factor receptors. *Cytokine & Growth Factor Reviews*, *16*(2), 139–149.
786 https://doi.org/10.1016/j.cytogfr.2005.01.001
787 Ferguson, H. R., Smith, M. P., & Francavilla, C. (2021). Fibroblast Growth Factor Receptors
788 (FGFRs) and Noncanonical Partners in Cancer Signaling. *Cells*, *10*(5), 1201.
789 https://doi.org/10.3390/cells10051201
790 Francavilla, C., & O'Brien, C. S. (2022). Fibroblast growth factor receptor signalling
791 dysregulation and targeting in breast cancer. *Open Biology*, *12*(2), 210373.
792 https://doi.org/10.1098/rsob.210373

793 Fukuyama, T., Ogita, H., Kawakatsu, T., Fukuhara, T., Yamada, T., Sato, T., Shimizu, K.,
794 Nakamura, T., Matsuda, M., & Takai, Y. (2005). Involvement of the c-Src-Crk-C3G-
795 Rap1 Signaling in the Nectin-induced Activation of Cdc42 and Formation of Adherens
796 Junctions. *Journal of Biological Chemistry*, *280*(1), 815–825.
797 https://doi.org/10.1074/jbc.M411099200
798 Fukuyama, T., Ogita, H., Kawakatsu, T., Inagaki, M., & Takai, Y. (2006). Activation of Rac by
799 cadherin through the c-Src–Rap1–phosphatidylinositol 3-kinase–Vav2 pathway.
800 *Oncogene*, *25*(1), 8–19. https://doi.org/10.1038/sj.onc.1209010
801 Giulianelli, S., Riggio, M., Guillardoy, T., Pérez Piñero, C., Gorostiaga, M. A., Sequeira, G.,
802 Pataccini, G., Abascal, M. F., Toledo, M. F., Jacobsen, B. M., Guerreiro, A. C., Barros,
803 A., Novaro, V., Monteiro, F. L., Amado, F., Gass, H., Abba, M., Helguero, L. A., &
804 Lanari, C. (2019). FGF2 induces breast cancer growth through ligand-independent
805 activation and recruitment of ERα and PRBΔ4 isoform to *MYC* regulatory sequences.
806 *International Journal of Cancer*, ijc.32252. https://doi.org/10.1002/ijc.32252
807 Gotoh, N. (2008). Regulation of growth factor signaling by FRS2 family docking/scaffold
808 adaptor proteins. *Cancer Science*, *99*(7), 1319–1325. https://doi.org/10.1111/j.1349-
809 7006.2008.00840.x
810 Grada, A., Otero-Vinas, M., Prieto-Castrillo, F., Obagi, Z., & Falanga, V. (2017). Research
811 Techniques Made Simple: Analysis of Collective Cell Migration Using the Wound
812 Healing Assay. *Journal of Investigative Dermatology*, *137*(2), e11–e16.
813 https://doi.org/10.1016/j.jid.2016.11.020

814 Gurzu, S., Kobori, L., Fodor, D., & Jung, I. (2019). Epithelial Mesenchymal and Endothelial
815 Mesenchymal Transitions in Hepatocellular Carcinoma: A Review. *BioMed Research*
816 *International*, *2019*, 1–12. https://doi.org/10.1155/2019/2962580
817 Hadari, Y. R., Kouhara, H., Lax, I., & Schlessinger, J. (1998). Binding of Shp2 Tyrosine
818 Phosphatase to FRS2 Is Essential for Fibroblast Growth Factor-Induced PC12 Cell
819 Differentiation. *Molecular and Cellular Biology*, *18*(7), 3966–3973.
820 https://doi.org/10.1128/MCB.18.7.3966
821 Hanahan, D., & Weinberg, R. A. (2011). Hallmarks of Cancer: The Next Generation. *Cell*,
822 *144*(5), 646–674. https://doi.org/10.1016/j.cell.2011.02.013
823 Houles, T., & Roux, P. P. (2018). Defining the role of the RSK isoforms in cancer. *Seminars in*
824 *Cancer Biology*, *48*, 53–61. https://doi.org/10.1016/j.semcancer.2017.04.016
825 Huang, Z., Tan, Y., Gu, J., Liu, Y., Song, L., Niu, J., Zhao, L., Srinivasan, L., Lin, Q., Deng, J.,
826 Li, Y., Conklin, D. J., Neubert, T. A., Cai, L., Li, X., & Mohammadi, M. (2017).
827 Uncoupling the Mitogenic and Metabolic Functions of FGF1 by Tuning FGF1-FGF
828 Receptor Dimer Stability. *Cell Reports*, *20*(7), 1717–1728.
829 https://doi.org/10.1016/j.celrep.2017.06.063
830 Jimenez-Morales, D., Rosa Campos, A., Von Dollen, J., Krogan, N., & Swaney, D. (2019).
831 *ArtMS: Analytical R tools for Mass Spectrometry*.
832 https://doi.org/doi:10.18129/B9.bioc.artMS
833 Karlsson, E., Waltersson, M. A., Bostner, J., Pérez-Tenorio, G., Olsson, B., Hallbeck, A.-L., &
834 Stål, O. (2011). High-resolution genomic analysis of the 11q13 amplicon in breast
835 cancers identifies synergy with 8p12 amplification, involving the mTOR targets S6K2

836 and 4EBP1. *Genes, Chromosomes and Cancer*, *50*(10), 775–787.
837 https://doi.org/10.1002/gcc.20900
838 Katoh, M., & Katoh, M. (2006). Cross-talk of WNT and FGF signaling pathways at GSK3ß to
839 regulate ß-catenin and SNAIL signaling cascades. *Cancer Biology & Therapy*, *5*(9),
840 1059–1064. https://doi.org/10.4161/cbt.5.9.3151
841 Katoh, M., & Nakagama, H. (2014). FGF Receptors: Cancer Biology and Therapeutics: cancer
842 biology and therapeutics on FGF receptors. *Medicinal Research Reviews*, *34*(2), 280–
843 300. https://doi.org/10.1002/med.21288
844 Kelher, M. R., McLaughlin, N. J. D., Banerjee, A., Elzi, D. J., Gamboni, F., Khan, S. Y., Meng,
845 X., Mitra, S., & Silliman, C. C. (2017). LysoPCs induce Hck- and PKCδ-mediated
846 activation of PKCγ causing p47 ^{phox} phosphorylation and membrane translocation in
847 neutrophils. *Journal of Leukocyte Biology*, *101*(1), 261–273.
848 https://doi.org/10.1189/jlb.3A0813-420RRR
849 Kim, H.-J., Kim, J.-H., Bae, S.-C., Choi, J.-Y., Kim, H.-J., & Ryoo, H.-M. (2003). The Protein
850 Kinase C Pathway Plays a Central Role in the Fibroblast Growth Factor-stimulated
851 Expression and Transactivation Activity of Runx2. *Journal of Biological Chemistry*,
852 *278*(1), 319–326. https://doi.org/10.1074/jbc.M203750200
853 Kiyatkin, A., van Alderwerelt van Rosenburgh, I. K., Klein, D. E., & Lemmon, M. A. (2020).
854 Kinetics of receptor tyrosine kinase activation define ERK signaling dynamics. *Science*
855 *Signaling*, *13*(645), eaaz5267. https://doi.org/10.1126/scisignal.aaz5267
856 Koledova, Z., Sumbal, J., Rabata, A., de La Bourdonnaye, G., Chaloupkova, R., Hrdlickova, B.,
857 Damborsky, J., & Stepankova, V. (2019). Fibroblast Growth Factor 2 Protein Stability
858 Provides Decreased Dependence on Heparin for Induction of FGFR Signaling and Alters

ERK Signaling Dynamics. *Frontiers in Cell and Developmental Biology*, *7*, 331. https://doi.org/10.3389/fcell.2019.00331

Korc, M., & Friesel, R. (2009). The Role of Fibroblast Growth Factors in Tumor Growth. *Current Cancer Drug Targets*, *9*(5), 639–651. https://doi.org/10.2174/156800909789057006

Korsten, S. G. P. J., Peracic, L., van Groeningen, L. M. B., Diks, M. A. P., Vromans, H., Garssen, J., & Willemsen, L. E. M. (2022). Butyrate Prevents Induction of CXCL10 and Non-Canonical IRF9 Expression by Activated Human Intestinal Epithelial Cells via HDAC Inhibition. *International Journal of Molecular Sciences*, *23*(7), 3980. https://doi.org/10.3390/ijms23073980

Kunath, T., Saba-El-Leil, M. K., Almousailleakh, M., Wray, J., Meloche, S., & Smith, A. (2007). FGF stimulation of the Erk1/2 signalling cascade triggers transition of pluripotent embryonic stem cells from self-renewal to lineage commitment. *Development*, *134*(16), 2895–2902. https://doi.org/10.1242/dev.02880

Kuo, C.-C., Savage, N. S., Chen, H., Wu, C.-F., Zyla, T. R., & Lew, D. J. (2014). Inhibitory GEF Phosphorylation Provides Negative Feedback in the Yeast Polarity Circuit. *Current Biology*, *24*(7), 753–759. https://doi.org/10.1016/j.cub.2014.02.024

Kuro-o, M. (2019). The Klotho proteins in health and disease. *Nature Reviews Nephrology*, *15*(1), 27–44. https://doi.org/10.1038/s41581-018-0078-3

Lavoie, H., Gagnon, J., & Therrien, M. (2020). ERK signalling: A master regulator of cell behaviour, life and fate. *Nature Reviews Molecular Cell Biology*, *21*(10), 607–632. https://doi.org/10.1038/s41580-020-0255-7

881 Liang, C.-C., Park, A. Y., & Guan, J.-L. (2007). In vitro scratch assay: A convenient and
882 inexpensive method for analysis of cell migration in vitro. *Nature Protocols*, *2*(2), 329–
883 333. https://doi.org/10.1038/nprot.2007.30
884 Lima, F., Niger, C., Hebert, C., & Stains, J. P. (2009). Connexin43 Potentiates Osteoblast
885 Responsiveness to Fibroblast Growth Factor 2 via a Protein Kinase C-Delta/Runx2–
886 dependent Mechanism. *Molecular Biology of the Cell*, *20*(11), 2697–2708.
887 https://doi.org/10.1091/mbc.e08-10-1079
888 Loog, M., & Morgan, D. O. (2005). Cyclin specificity in the phosphorylation of cyclin-
889 dependent kinase substrates. *Nature*, *434*(7029), 104–108.
890 https://doi.org/10.1038/nature03329
891 Looi, C.-K., Hii, L.-W., Ngai, S. C., Leong, C.-O., & Mai, C.-W. (2020). The Role of Ras-
892 Associated Protein 1 (Rap1) in Cancer: Bad Actor or Good Player? *Biomedicines*, *8*(9),
893 334. https://doi.org/10.3390/biomedicines8090334
894 Lovicu, F. J., & McAvoy, J. W. (2001). FGF-induced ERK activation in the lens. *Development*,
895 *128*(5075–5084), 10. https://doi.org/10.1242/dev.128.24.5075
896 Maher, P. (1999). P38 Mitogen-activated Protein Kinase Activation Is Required for Fibroblast
897 Growth Factor-2-stimulated Cell Proliferation but Not Differentiation. *Journal of*
898 *Biological Chemistry*, *274*(25), 17491–17498. https://doi.org/10.1074/jbc.274.25.17491
899 Marquette, A., André, J., Bagot, M., Bensussan, A., & Dumaz, N. (2011). ERK and PDE4
900 cooperate to induce RAF isoform switching in melanoma. *Nature Structural & Molecular*
901 *Biology*, *18*(5), 584–591. https://doi.org/10.1038/nsmb.2022
902 Maurer, G., Tarkowski, B., & Baccarini, M. (2011). Raf kinases in cancer–roles and therapeutic
903 opportunities. *Oncogene*, *30*(32), 3477–3488. https://doi.org/10.1038/onc.2011.160

Metzner, T., Bedeir, A., Held, G., Peter-Vörösmarty, B., Ghassemi, S., Heinzle, C., Spiegl-Kreinecker, S., Marian, B., Holzmann, K., Grasl-Kraupp, B., Pirker, C., Micksche, M., Berger, W., Heffeter, P., & Grusch, M. (2011). Fibroblast Growth Factor Receptors as Therapeutic Targets in Human Melanoma: Synergism with BRAF Inhibition. *Journal of Investigative Dermatology*, *131*(10), 2087–2095. https://doi.org/10.1038/jid.2011.177

Mohammadi, M., Jaye, M., Rubinstein, M., & Schlessinger, J. (1991). A Tyrosine-Phosphorylated Carboxy-Terminal Peptide of the Fibroblast Growth Factor Receptor (Flg) Is a Binding Site for the SH2 Domain of Phospholipase C--yl. *VOL* ., 11.

Morris, M. K., Saez-Rodriguez, J., Sorger, P. K., & Lauffenburger, D. A. (2010). Logic-Based Models for the Analysis of Cell Signaling Networks. *Biochemistry*, *49*(15), 3216–3224. https://doi.org/10.1021/bi902202q

New, L. (1998). PRAK, a novel protein kinase regulated by the p38 MAP kinase. *The EMBO Journal*, *17*(12), 3372–3384. https://doi.org/10.1093/emboj/17.12.3372

Niger, C., Hebert, C., & Stains, J. P. (2010). Interaction of connexin43 and protein kinase C-delta during FGF2 signaling. *BMC Biochemistry*, *11*(1), 14. https://doi.org/10.1186/1471-2091-11-14

Nolen, B., Taylor, S., & Ghosh, G. (2004). Regulation of Protein Kinases: Controlling Activity through Activation Segment Conformation. *Molecular Cell*, *15*(5), 661–675. https://doi.org/10.1016/j.molcel.2004.08.024

Ornitz, D. M., & Itoh, N. (2015). The Fibroblast Growth Factor signaling pathway. *WIREs Developmental Biology*, *4*(3), 215–266. https://doi.org/10.1002/wdev.176

Ornitz, D. M., & Itoh, N. (2022). New developments in the biology of fibroblast growth factors. *WIREs Mechanisms of Disease*, *14*(4). https://doi.org/10.1002/wsbm.1549

927 Ornitz, D. M., Xu, J., Colvin, J. S., McEwen, D. G., MacArthur, C. A., Coulier, F., Gao, G., &
928 Goldfarb, M. (1996). Receptor Specificity of the Fibroblast Growth Factor Family.
929 *Journal of Biological Chemistry*, *271*(25), 15292–15297.
930 https://doi.org/10.1074/jbc.271.25.15292
931 Pino, L. K., Searle, B. C., Bollinger, J. G., Nunn, B., MacLean, B., & MacCoss, M. J. (2020).
932 The Skyline ecosystem: Informatics for quantitative mass spectrometry proteomics. *Mass*
933 *Spectrometry Reviews*, *39*(3), 229–244. https://doi.org/10.1002/mas.21540
934 Post, H., Penning, R., Fitzpatrick, M. A., Garrigues, L. B., Wu, W., MacGillavry, H. D.,
935 Hoogenraad, C. C., Heck, A. J. R., & Altelaar, A. F. M. (2017). Robust, Sensitive, and
936 Automated Phosphopeptide Enrichment Optimized for Low Sample Amounts Applied to
937 Primary Hippocampal Neurons. *Journal of Proteome Research*, *16*(2), 728–737.
938 https://doi.org/10.1021/acs.jproteome.6b00753
939 Presta, M., Chiodelli, P., Giacomini, A., Rusnati, M., & Ronca, R. (2017). Fibroblast growth
940 factors (FGFs) in cancer: FGF traps as a new therapeutic approach. *Pharmacology &*
941 *Therapeutics*, *179*, 171–187. https://doi.org/10.1016/j.pharmthera.2017.05.013
942 Qu, J., Cammarano, M. S., Shi, Q., Ha, K. C., de Lanerolle, P., & Minden, A. (2001). Activated
943 PAK4 Regulates Cell Adhesion and Anchorage-Independent Growth. *Molecular and*
944 *Cellular Biology*, *21*(10), 3523–3533. https://doi.org/10.1128/MCB.21.10.3523-
945 3533.2001
946 Raina, D., Fabris, F., Morelli, L. G., & Schröter, C. (2022). Intermittent ERK oscillations
947 downstream of FGF in mouse embryonic stem cells. *Development*, *149*(4), dev199710.
948 https://doi.org/10.1242/dev.199710

949 Ramos, C., Becerril, C., Montaño, M., García-De-Alba, C., Ramírez, R., Checa, M., Pardo, A., &
950 Selman, M. (2010). FGF-1 reverts epithelial-mesenchymal transition induced by TGF-β1
951 through MAPK/ERK kinase pathway. *American Journal of Physiology-Lung Cellular*
952 *and Molecular Physiology*, *299*(2), L222–L231.
953 https://doi.org/10.1152/ajplung.00070.2010
954 Ramos-Alvarez, I., & Jensen, R. T. (2018). P21-activated kinase 4 in pancreatic acinar cells is
955 activated by numerous gastrointestinal hormones/neurotransmitters and growth factors by
956 novel signaling, and its activation stimulates secretory/growth cascades. *American*
957 *Journal of Physiology-Gastrointestinal and Liver Physiology*, *315*(2), G302–G317.
958 https://doi.org/10.1152/ajpgi.00005.2018
959 Ranieri, D., Nanni, M., Persechino, F., Torrisi, M. R., & Belleudi, F. (2020). Role of PKCε in the
960 epithelial-mesenchymal transition induced by FGFR2 isoform switch. *Cell*
961 *Communication and Signaling*, *18*(1), 76. https://doi.org/10.1186/s12964-020-00582-1
962 Rehmann, H., Das, J., Knipscheer, P., Wittinghofer, A., & Bos, J. L. (2006). Structure of the
963 cyclic-AMP-responsive exchange factor Epac2 in its auto-inhibited state. *Nature*,
964 *439*(7076), 625–628. https://doi.org/10.1038/nature04468
965 Rehmann, H., Prakash, B., Wolf, E., Rueppel, A., de Rooij, J., Bos, J. L., & Wittinghofer, A.
966 (2003). Structure and regulation of the cAMP-binding domains of Epac2. *Nature*
967 *Structural Biology*, *10*(1), 26–32. https://doi.org/10.1038/nsb878
968 Romeo, Y., Zhang, X., & Roux, P. P. (2012). Regulation and function of the RSK family of
969 protein kinases. *Biochemical Journal*, *441*(2), 553–569.
970 https://doi.org/10.1042/BJ20110289

971 Saini, K. S., Loi, S., de Azambuja, E., Metzger-Filho, O., Saini, M. L., Ignatiadis, M., Dancey, J.
972 E., & Piccart-Gebhart, M. J. (2013). Targeting the PI3K/AKT/mTOR and Raf/MEK/ERK
973 pathways in the treatment of breast cancer. *Cancer Treatment Reviews*, *39*(8), 935–946.
974 https://doi.org/10.1016/j.ctrv.2013.03.009
975 Sarabipour, S., & Hristova, K. (2016). Mechanism of FGF receptor dimerization and activation.
976 *Nature Communications*, *7*(1), 10262. https://doi.org/10.1038/ncomms10262
977 Schindelin, J., Arganda-Carreras, I., Frise, E., Kaynig, V., Longair, M., Pietzsch, T., Preibisch,
978 S., Rueden, C., Saalfeld, S., Schmid, B., Tinevez, J.-Y., White, D. J., Hartenstein, V.,
979 Eliceiri, K., Tomancak, P., & Cardona, A. (2012). Fiji: An open-source platform for
980 biological-image analysis. *Nature Methods*, *9*(7), 676–682.
981 https://doi.org/10.1038/nmeth.2019
982 Schmidlin, T., Debets, D. O., Gelder, C. A. G. H. van, Stecker, K. E., Rontogianni, S., Eshof, B.
983 L. van den, Kemper, K., Lips, E. H., Biggelaar, M. van den, Peeper, D. S., Heck, A. J. R.,
984 & Altelaar, M. (2019). High-Throughput Assessment of Kinome-wide Activation States.
985 *Cell Systems*, *9*(4), 366-374.e5. https://doi.org/10.1016/j.cels.2019.08.005
986 Schmitt, J. M., & Stork, P. J. S. (2002). PKA Phosphorylation of Src Mediates cAMP's
987 Inhibition of Cell Growth via Rap1. *Molecular Cell*, *9*(1), 85–94.
988 https://doi.org/10.1016/S1097-2765(01)00432-4
989 Shalaby, A. A., Presneau, N., Idowu, B. D., Thompson, L., Briggs, T. R., Tirabosco, R., Diss, T.
990 C., & Flanagan, A. M. (2009). Analysis of the fibroblastic growth factor receptor-
991 RAS/RAF/MEK/ERK-ETS2/brachyury signalling pathway in chordomas. *Modern*
992 *Pathology*, *22*(8), 996–1005. https://doi.org/10.1038/modpathol.2009.63

993 Sharpe, R., Pearson, A., Herrera-Abreu, M. T., Johnson, D., Mackay, A., Welti, J. C., Natrajan,
994 R., Reynolds, A. R., Reis-Filho, J. S., Ashworth, A., & Turner, N. C. (2011). FGFR
995 Signaling Promotes the Growth of Triple-Negative and Basal-Like Breast Cancer Cell
996 Lines Both *In Vitro* and *In Vivo*. *Clinical Cancer Research*, *17*(16), 5275–5286.
997 https://doi.org/10.1158/1078-0432.CCR-10-2727
998 Shi, W., Peyrot, S. M., Munro, E., & Levine, M. (2009). FGF3 in the floor plate directs
999 notochord convergent extension in the *Ciona* tadpole. *Development*, *136*(1), 23–28.
1000 https://doi.org/10.1242/dev.029157
1001 Shin, S.-Y., Rath, O., Choo, S.-M., Fee, F., McFerran, B., Kolch, W., & Cho, K.-H. (2009).
1002 Positive- and negative-feedback regulations coordinate the dynamic behavior of the Ras-
1003 Raf-MEK-ERK signal transduction pathway. *Journal of Cell Science*, *122*(3), 425–435.
1004 https://doi.org/10.1242/jcs.036319
1005 Shinya, M., Koshida, S., Sawada, A., Kuroiwa, A., & Takeda, H. (2001). Fgf signalling through
1006 MAPK cascade is required for development of the subpallial telencephalon in zebrafish
1007 embryos. *Development*, *128*(21), 4153–4164. https://doi.org/10.1242/dev.128.21.4153
1008 Smith, M. P., Ferguson, H. R., Ferguson, J., Zindy, E., Kowalczyk, K. M., Kedward, T., Bates,
1009 C., Parsons, J., Watson, J., Chandler, S., Fullwood, P., Warwood, S., Knight, D., Clarke,
1010 R. B., & Francavilla, C. (2021). *Reciprocal Priming between Receptor Tyrosine Kinases*
1011 *at Recycling Endosomes Orchestrates Cellular Signalling Outputs* [Preprint]. Cell
1012 Biology. https://doi.org/10.1101/2021.01.04.425243
1013 Sonntag, T., Moresco, J. J., Vaughan, J. M., Matsumura, S., Yates, J. R., & Montminy, M.
1014 (2017). Analysis of a cAMP regulated coactivator family reveals an alternative

phosphorylation motif for AMPK family members. *PLOS ONE*, *12*(2), e0173013. https://doi.org/10.1371/journal.pone.0173013

Spivak-Kroizman, T., Lemmon, M. A., Dikic, I., Ladbury, J. E., Pinchasi, D., Huang, J., Jaye, M., Crumley, G., Schlessinger, J., & Lax, I. (1994). Heparin-induced oligomerization of FGF molecules is responsible for FGF receptor dimerization, activation, and cell proliferation. *Cell*, *79*(6), 1015–1024. https://doi.org/10.1016/0092-8674(94)90032-9

Stokman, G., Qin, Y., Booij, T. H., Ramaiahgari, S., Lacombe, M., Dolman, M. E. M., van Dorenmalen, K. M. A., Teske, G. J. D., Florquin, S., Schwede, F., van de Water, B., Kok, R. J., & Price, L. S. (2014). Epac-Rap Signaling Reduces Oxidative Stress in the Tubular Epithelium. *Journal of the American Society of Nephrology*, *25*(7), 1474–1485. https://doi.org/10.1681/ASN.2013070679

Stuart, S. A., Houel, S., Lee, T., Wang, N., Old, W. M., & Ahn, N. G. (2015). A Phosphoproteomic Comparison of B-RAFV600E and MKK1/2 Inhibitors in Melanoma Cells*. *Molecular & Cellular Proteomics*, *14*(6), 1599–1615. https://doi.org/10.1074/mcp.M114.047233

Su, N., Jin, M., & Chen, L. (2014). Role of FGF/FGFR signaling in skeletal development and homeostasis: Learning from mouse models. *Bone Research*, *2*(1), 14003. https://doi.org/10.1038/boneres.2014.3

Suarez-Arnedo, A., Torres Figueroa, F., Clavijo, C., Arbeláez, P., Cruz, J. C., & Muñoz-Camargo, C. (2020). An image J plugin for the high throughput image analysis of in vitro scratch wound healing assays. *PLOS ONE*, *15*(7), e0232565. https://doi.org/10.1371/journal.pone.0232565

1037 Subramanian, A., Tamayo, P., Mootha, V. K., Mukherjee, S., Ebert, B. L., Gillette, M. A.,
1038 Paulovich, A., Pomeroy, S. L., Golub, T. R., Lander, E. S., & Mesirov, J. P. (2005). Gene
1039 set enrichment analysis: A knowledge-based approach for interpreting genome-wide
1040 expression profiles. *Proceedings of the National Academy of Sciences*, *102*(43), 15545–
1041 15550. https://doi.org/10.1073/pnas.0506580102
1042 Sun, P., Yoshizuka, N., New, L., Moser, B. A., Li, Y., Liao, R., Xie, C., Chen, J., Deng, Q.,
1043 Yamout, M., Dong, M.-Q., Frangou, C. G., Yates, J. R., Wright, P. E., & Han, J. (2007).
1044 PRAK Is Essential for ras-Induced Senescence and Tumor Suppression. *Cell*, *128*(2),
1045 295–308. https://doi.org/10.1016/j.cell.2006.11.050
1046 Sun, Y., Fan, X., Zhang, Q., Shi, X., Xu, G., & Zou, C. (2017). Cancer-associated fibroblasts
1047 secrete FGF-1 to promote ovarian proliferation, migration, and invasion through the
1048 activation of FGF-1/FGFR4 signaling. *Tumor Biology*, *39*(7), 101042831771259.
1049 https://doi.org/10.1177/1010428317712592
1050 Szybowska, P., Kostas, M., Wesche, J., Haugsten, E. M., & Wiedlocha, A. (2021). Negative
1051 Regulation of FGFR (Fibroblast Growth Factor Receptor) Signaling. *Cells*, *10*(6), 1342.
1052 https://doi.org/10.3390/cells10061342
1053 Taylor, S. C., Nadeau, K., Abbasi, M., Lachance, C., Nguyen, M., & Fenrich, J. (2019). The
1054 Ultimate qPCR Experiment: Producing Publication Quality, Reproducible Data the First
1055 Time. *Trends in Biotechnology*, *37*(7), 761–774.
1056 https://doi.org/10.1016/j.tibtech.2018.12.002
1057 Teng, Y., Guo, B., Mu, X., & Liu, S. (2018). KIF26B promotes cell proliferation and migration
1058 through the FGF2/ERK signaling pathway in breast cancer. *Biomedicine &*
1059 *Pharmacotherapy*, *108*, 766–773. https://doi.org/10.1016/j.biopha.2018.09.036

Terfve, C., Cokelaer, T., Henriques, D., MacNamara, A., Goncalves, E., Morris, M. K., Iersel, M. van, Lauffenburger, D. A., & Saez-Rodriguez, J. (2012). CellNOptR: A flexible toolkit to train protein signaling networks to data using multiple logic formalisms. *BMC Systems Biology*, *6*(1), 133. https://doi.org/10.1186/1752-0509-6-133

Thillai, K., Lam, H., Sarker, D., & Wells, C. M. (2017). Deciphering the link between PI3K and PAK: An opportunity to target key pathways in pancreatic cancer? *Oncotarget*, *8*(8), 14173–14191. https://doi.org/10.18632/oncotarget.13309

Tognetti, M., Gabor, A., Yang, M., Cappelletti, V., Windhager, J., Rueda, O. M., Charmpi, K., Esmaeilishirazifard, E., Bruna, A., de Souza, N., Caldas, C., Beyer, A., Picotti, P., Saez-Rodriguez, J., & Bodenmiller, B. (2021). Deciphering the signaling network of breast cancer improves drug sensitivity prediction. *Cell Systems*, *12*(5), 401-418.e12. https://doi.org/10.1016/j.cels.2021.04.002

Tomita, H., Tanaka, K., Hirata, A., Okada, H., Imai, H., Shirakami, Y., Ohnishi, K., Sugie, S., Aoki, H., Hatano, Y., Noguchi, K., Kanayama, T., Niwa, A., Suzui, N., Miyazaki, T., Tanaka, T., Akiyama, H., Shimizu, M., Yoshida, K., & Hara, A. (2021). Inhibition of FGF10-ERK signal activation suppresses intraductal papillary neoplasm of the bile duct and its associated carcinomas. *Cell Reports*, *34*(8), 108772. https://doi.org/10.1016/j.celrep.2021.108772

Touat, M., Ileana, E., Postel-Vinay, S., André, F., & Soria, J.-C. (2015). Targeting FGFR Signaling in Cancer. *Clinical Cancer Research*, *21*(12), 2684–2694. https://doi.org/10.1158/1078-0432.CCR-14-2329

1081 Türei, D., Korcsmáros, T., & Saez-Rodriguez, J. (2016). OmniPath: Guidelines and gateway for
1082 literature-curated signaling pathway resources. *Nature Methods*, *13*(12), 966–967.
1083 https://doi.org/10.1038/nmeth.4077
1084 Tyanova, S., Temu, T., & Cox, J. (2016). The MaxQuant computational platform for mass
1085 spectrometry-based shotgun proteomics. *Nature Protocols*, *11*(12), 2301–2319.
1086 https://doi.org/10.1038/nprot.2016.136
1087 Valverde, J., Altelaar, A. F. M., Dubra, G., Toorn, H. W. P. V. den, Mierlo, G. van, Vermeulen,
1088 M., Heck, A., Elena-Real, C., Fournet, A., Ghoul, E. A., Chahar, D., Haider, A., Paloni,
1089 M., Constantinou, A., Barducci, A., Ghosh, K., Sibille, N., Bernadó, P., Knipscheer, P.,
1090 … Fisher, D. (2022). *A CDK-mediated phosphorylation switch of disordered protein*
1091 *condensation* [Preprint]. In Review. https://doi.org/10.21203/rs.3.rs-1370895/v1
1092 Vasaikar, S. V., Deshmukh, A. P., den Hollander, P., Addanki, S., Kuburich, N. A., Kudaravalli,
1093 S., Joseph, R., Chang, J. T., Soundararajan, R., & Mani, S. A. (2021). EMTome: A
1094 resource for pan-cancer analysis of epithelial-mesenchymal transition genes and
1095 signatures. *British Journal of Cancer*, *124*(1), 259–269. https://doi.org/10.1038/s41416-
1096 020-01178-9
1097 Wang, W., Chen, T., Li, H., Chen, Y., Wu, Z., Feng, T., Zhang, X., Zhong, Q., Zhong, Q., Li, G.,
1098 Guo, L., Zhou, L., & Zhou, J. (2015). Screening a novel FGF3 antagonist peptide with
1099 anti-tumor effects on breast cancer from a phage display library. *Molecular Medicine*
1100 *Reports*, *12*(5), 7051–7058. https://doi.org/10.3892/mmr.2015.4248
1101 Wang, Y., Wang, W., Wu, H., Zhou, Y., Qin, X., Wang, Y., Wu, J., Sun, X.-Y., Yang, Y., Xu,
1102 H., Qian, X., Pang, X., Li, Y., Zhang, Z., Han, J., & Zhang, Y. (2021). The essential role

of PRAK in tumor metastasis and its therapeutic potential. *Nature Communications*, *12*(1), 1736. https://doi.org/10.1038/s41467-021-21993-9

Watson, J., & Francavilla, C. (2018). Regulation of FGF10 Signaling in Development and Disease. *Frontiers in Genetics*, *9*, 500. https://doi.org/10.3389/fgene.2018.00500

Wellbrock, C., Karasarides, M., & Marais, R. (2004). The RAF proteins take centre stage. *Nature Reviews Molecular Cell Biology*, *5*(11), 875–885. https://doi.org/10.1038/nrm1498

Wittmann, D. M., Krumsiek, J., Saez-Rodriguez, J., Lauffenburger, D. A., Klamt, S., & Theis, F. J. (2009). Transforming Boolean models to continuous models: Methodology and application to T-cell receptor signaling. *BMC Systems Biology*, *3*(1), 98. https://doi.org/10.1186/1752-0509-3-98

Wolf, I., Levanon-Cohen, S., Bose, S., Ligumsky, H., Sredni, B., Kanety, H., Kuro-o, M., Karlan, B., Kaufman, B., Koeffler, H. P., & Rubinek, T. (2008). Klotho: A tumor suppressor and a modulator of the IGF-1 and FGF pathways in human breast cancer. *Oncogene*, *27*(56), 7094–7105. https://doi.org/10.1038/onc.2008.292

Won, S.-Y., Park, J.-J., Shin, E.-Y., & Kim, E.-G. (2019). PAK4 signaling in health and disease: Defining the PAK4–CREB axis. *Experimental & Molecular Medicine*, *51*(2), 1–9. https://doi.org/10.1038/s12276-018-0204-0

Xie, Y., Su, N., Yang, J., Tan, Q., Huang, S., Jin, M., Ni, Z., Zhang, B., Zhang, D., Luo, F., Chen, H., Sun, X., Feng, J. Q., Qi, H., & Chen, L. (2020). FGF/FGFR signaling in health and disease. *Signal Transduction and Targeted Therapy*, *5*(1), 181. https://doi.org/10.1038/s41392-020-00222-7

Yan, C., Grimm, W. A., Garner, W. L., Qin, L., Travis, T., Tan, N., & Han, Y.-P. (2010). Epithelial to Mesenchymal Transition in Human Skin Wound Healing Is Induced by Tumor Necrosis Factor-α through Bone Morphogenic Protein-2. *The American Journal of Pathology*, *176*(5), 2247–2258. https://doi.org/10.2353/ajpath.2010.090048

Yang, W., Klaman, L. D., Chen, B., Araki, T., Harada, H., Thomas, S. M., George, E. L., & Neel, B. G. (2006). An Shp2/SFK/Ras/Erk Signaling Pathway Controls Trophoblast Stem Cell Survival. *Developmental Cell*, *10*(3), 317–327. https://doi.org/10.1016/j.devcel.2006.01.002

Zang, M., Gong, J., Luo, L., Zhou, J., Xiang, X., Huang, W., Huang, Q., Luo, X., Olbrot, M., Peng, Y., Chen, C., & Luo, Z. (2008). Characterization of Ser338 Phosphorylation for Raf-1 Activation. *Journal of Biological Chemistry*, *283*(46), 31429–31437. https://doi.org/10.1074/jbc.M802855200

Zhang, C., Yang, T., & Jiang, H. (2020). MiR-511 inhibits proliferation and metastasis of breast cancer cells by targeting FGF4. *The Journal of Gene Medicine*, *22*(9). https://doi.org/10.1002/jgm.3168

Zhang, X., Ibrahimi, O. A., Olsen, S. K., Umemori, H., Mohammadi, M., & Ornitz, D. M. (2006). Receptor Specificity of the Fibroblast Growth Factor Family. *Journal of Biological Chemistry*, *281*(23), 15694–15700. https://doi.org/10.1074/jbc.M601252200

Zhao, X., Xu, F., Dominguez, N. P., Xiong, Y., Xiong, Z., Peng, H., Shay, C., & Teng, Y. (2018). FGFR4 provides the conduit to facilitate FGF19 signaling in breast cancer progression. *Molecular Carcinogenesis*, *57*(11), 1616–1625. https://doi.org/10.1002/mc.22884

1147 Zhou, B. P., Deng, J., Xia, W., Xu, J., Li, Y. M., Gunduz, M., & Hung, M.-C. (2004). Dual
1148 regulation of Snail by GSK-3β-mediated phosphorylation in control of epithelial–
1149 mesenchymal transition. *Nature Cell Biology*, *6*(10), 931–940.
1150 https://doi.org/10.1038/ncb1173
1151 Zhou, Y., Wu, C., Lu, G., Hu, Z., Chen, Q., & Du, X. (2020). FGF/FGFR signaling pathway
1152 involved resistance in various cancer types. *Journal of Cancer*, *11*(8), 2000–2007.
1153 https://doi.org/10.7150/jca.40531

1154

1155 ## Supplemental information

1156 **Supplementary Figure 1: Kinome activity after FGF stimulation in breast cancer.**

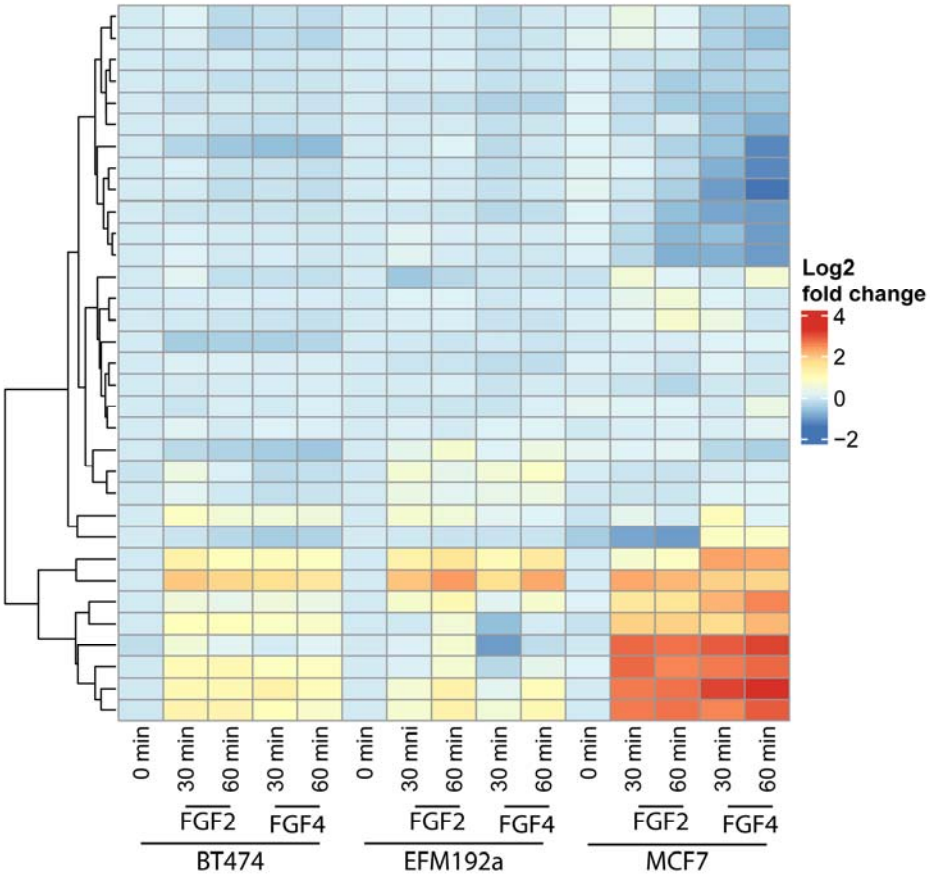

1157

Supplementary Figure 1: Kinome activity after FGF stimulation in breast cancer cells. MCF-7, BT-474, and EFM-192a cells were stimulated with 50ng/mL of either FGF2 or FGF4 supplemented with 5µg/mL of heparin. After 0, 30, and 60 minutes, the cells were harvested and subjected to measurement using the targeted kinome assay. The heatmap shows the quantified activation-determining phosphorylated sites on the kinases (biological triplicates). Only significantly changing values are shown (ANOVA $p < 0.05$).

Supplementary Figure 2: qPCR quantification of FGFR abundance.

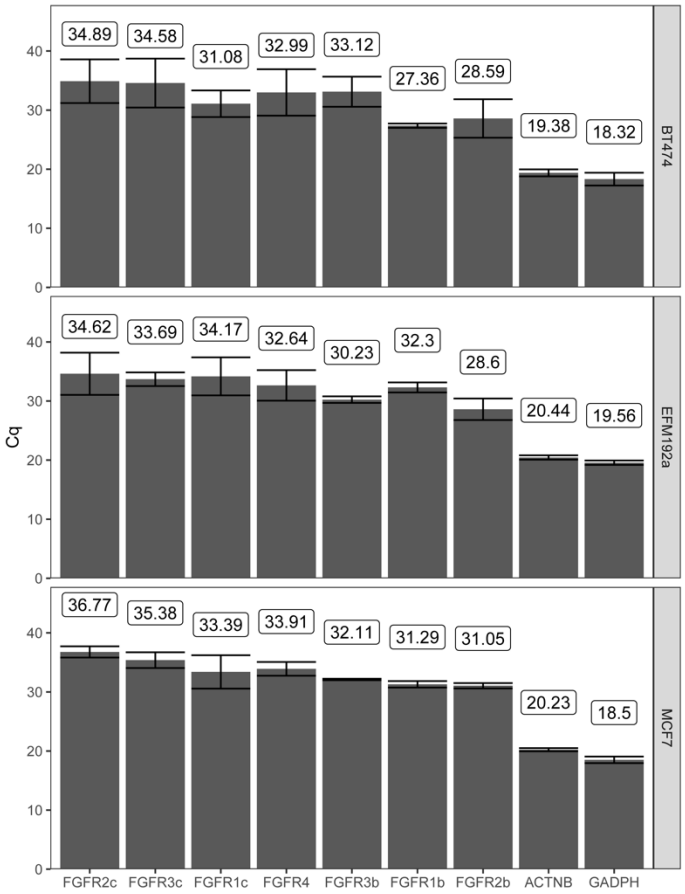

Supplementary Figure 2: qPCR quantification of FGFR abundance. FGFR expression levels were quantified using qPCR in MCF-7, BT-474, and EFM-192a cells using FGFR subtype-specific primers (triplicate measurements) (**Supplementary table 5**). Beta-actin and Glyceraldehyde-3-phosphate dehydrogenase was quantified to enable normalization across cell types. Reported values are the quantitation cycles (Cq) that negatively correlates with the RNA expression levels.

Supplementary Figure 3: FGF-induced MARK kinase regulation.

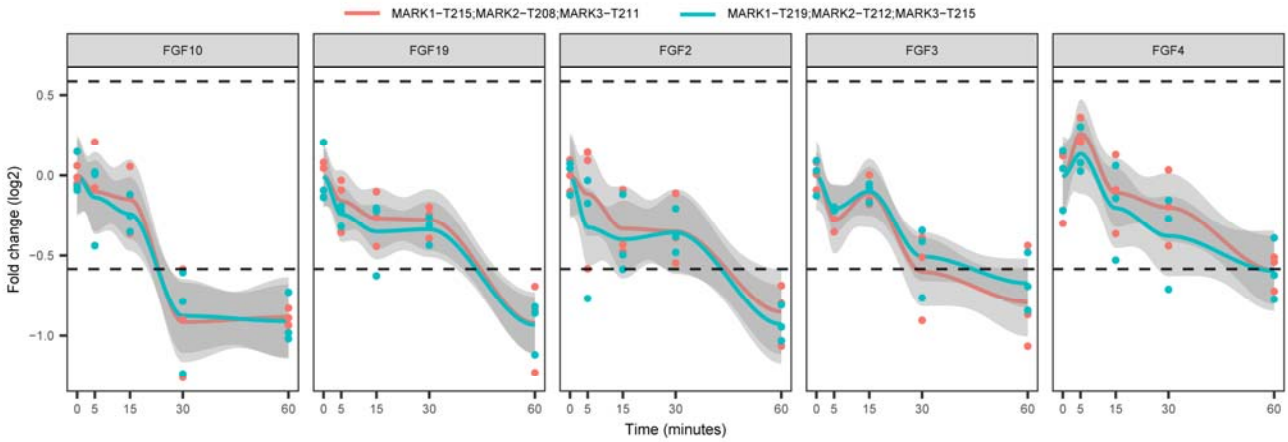

Supplementary Figure 3: FGF induced MARK kinase regulation. Activity-determining phosphorylation in the activation loop of MARK1, MARK2, and MARK3 was quantified in MCF-7 treated with different FGF ligands. Line plots show these quantified phosphorylated sites (biological triplicates). Values are represented in log2 and the 1.5 fold-change is represented using the dashed line.

Supplementary Figure 4: proteome derived EMT signature.

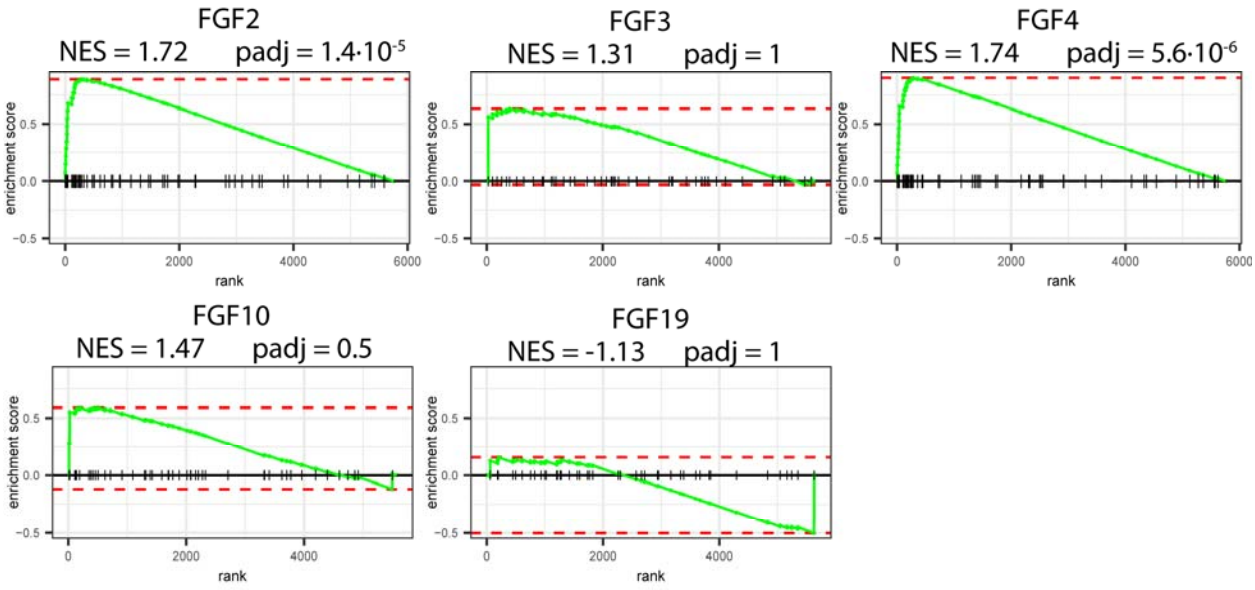

Supplementary figure 4: proteome derived EMT signature. MCF-7 cells treated were treated for 24 hours with the FGF ligands and their proteomes quantified. Subsequently, GSEA analysis on these proteomes (biological triplicates) was performed using the

MsigDB signature "HALLMARK_EPITHELIAL_MESENCHYMAL_TRANSITION". The normalized enrichment score (NES) along with the adjusted p-value is reported.

Supplementary Figure 5: Regulation of kinases implicated in PLCγ signaling.

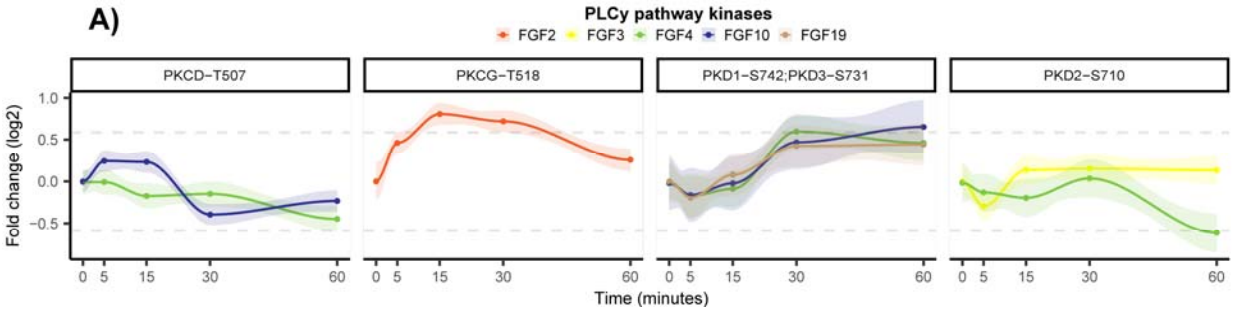

Supplementary Figure 5: Regulation of kinases implicated in PLCγ signaling A) Kinome activity was quantified of MCF-7 cells treated with 50ng/mL of either FGF2, FGF3, FGF4, FGF10, or FGF19, together with 5µg/mL of heparin. Only the activity dynamics of significantly regulated kinases (biological triplicates, ANOVA $p < 0.05$) from the PLCγ pathway are plotted. Grey lines represent a 1.5 fold-change, and 90% confidence intervals are presented per quantified phosphorylated peptide.

Supplementary Figure 6: RAP1 pulldown on FGF-stimulated cells.

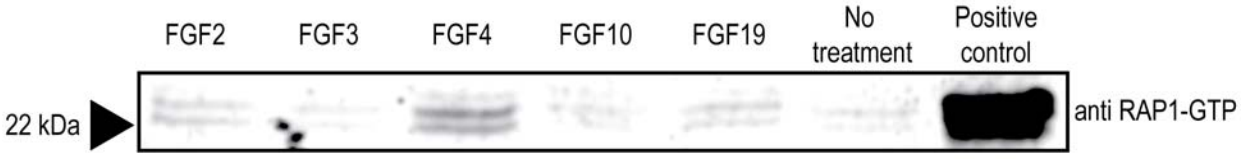

Supplementary Figure 6: RAP1 pulldown on FGF-stimulated cells. MCF-7 cells were stimulated with either FGF2, FGF3, FGF4, FGF10, and FGF19. Also, a no-stimulation control and a positive control were included. The negative control constituted unstimulated MCF-7 cells. The positive control constituted MCF-7 cell lysate with activated RAP1 by incubating the lysate with GTPγS, which activates all RAP1 in the lysate. The assay consisted of a pulldown of GTP-bound (active) Rap1 of equal amounts of proteins, followed by a western blot using an α–RAP1-GTP antibody.